UC Berkeley
UC Berkeley Electronic Theses and Dissertations

Title
Programmable Manipulation of Adherent Cell Motility Using Biological Breadboards

Permalink
https://escholarship.org/uc/item/6k22z243

Author
Yoon, Sang-Hee

Publication Date
2010

Peer reviewed|Thesis/dissertation

eScholarship.org Powered by the California Digital Library
University of California

Programmable Manipulation of Adherent Cell Motility Using Biological Breadboards

by

Sang-Hee Yoon

A dissertation submitted in partial satisfaction of the

requirements for the degree of

Doctor of Philosophy

in

Engineering – Mechanical Engineering

in the

Graduate Division

of the

University of California, Berkeley

Committee in charge:

Professor Mohammad R. K. Mofrad, Co-chair
Professor Dorian Liepmann, Co-chair
Professor Stanley A. Berger
Professor Seung-Wuk Lee

Fall 2010

Abstract

Programmable Manipulation of Adherent Cell Motility Using Biological Breadboards

by

Sang-Hee Yoon

Doctor of Philosophy in Mechanical Engineering

University of California, Berkeley

Professor Mohammad R. K. Mofrad, Co-chair
Professor Dorian Liepmann, Co-chair

The dynamic nature of cellular attachment and detachment which regulates cell function must be characterized to understand essential biological phenomena such as embryonic development, inflammatory immune response, wound repair, cancer metastasis, etc. Although extensive efforts have been devoted toward cell motility manipulation for a better understanding cellular dynamics, these efforts have remained in their infancy. A programmable manipulation of adherent-cell motility therefore has remained a challenging task. The goal of this research is to design addressable, multi-functional, and reusable biological platforms, nicknamed *biological breadboards (BBBs)*, to enable the spatiotemporal manipulation of cell motility at cellular and even subcellular levels, offering a new method to analyze cellular dynamics in a quantitative way. In this thesis, this method for cell motility manipulation using BBBs and their applications to quantitative characterizations of single-cellular and intracellular dynamics are summarized.

The BBBs consisting of M×N gold electrodes, identical and independently operated, on Pyrex glass substrate are designed to secure their addressability, thereby achieving a high-degree-of-freedom in programmable manipulation of adherent cell motility. This programmable manipulation of adherent cell motility is implicated by two fundamental mechanisms of cell attachment and detachment. An arginine-glycine-aspartic (RGD) acid-terminated thiol is introduced to achieve those mechanisms by tethering the RGD to the gold electrodes via thiol linker. The first mechanism is solved by a RGD which is a recognition sequence for integrin binding to many extracellular matrix proteins. The RGD-terminated thiol connects a RGD peptide into the gold electrodes using its thiol end which shows a spontaneous chemisorption of $\text{R-S-H} + \text{Au} \rightarrow \text{R-S-Au} + 1/2\,\text{H}_2$ where R is a substituent, thereby enhancing cell adhesion on the BBB. The second mechanism depends on a rapid reductive desorption of the thiol-gold self-assembled monolayer under negative bias voltage, $\text{R-S-Au} + \text{H}^+ + \text{e}^- \rightarrow \text{R-S-H} + \text{Au}$. This reaction makes the RGD-terminated thiol and even a cell or a part of the cell thereon detached from the gold electrodes. The BBBs are fabricated with microfabrication processes (optical lithography, e-beam evaporation, and

treatment on Pyrex glass and RGD-terminated thiol treatment on gold electrodes. The first is intended to achieve a cell-resistive surface which suppresses cell spreading on them, whereas the second is planned to tether a RGD peptide into gold via thiol linker, thereby providing a cell-adhesive surface.

In the experimental studies with a mouse embryonic fibroblast cell line (NIH 3T3), cellular and subcellular detachments have been made with the fabricated BBBs both to quantitatively characterize cellular and subcellular detachment dynamics and to investigate the addressability, multi-functionality, and reusability of the BBBs, thereby evaluating the BBBs as biological platforms for programmable manipulation of adherent cell motility. In addition, the changes in viscoelastic properties of the detached and retracting thin layer of a NIH 3T3 cell have been investigated.

Table of Contents

LIST OF FIGURES

NOMENCLATURE

Alphabetic letters

a	Area
Ag	Silver
Au	Gold
c	Damping coefficient
C	Carbon
Cl	Chlorine
CO_2	Carbon dioxide
Cr	Chromium
H	Hydrogen
H	Heaviside function
H_2O_2	Hydrogen peroxide
H_2SO_4	Sulfuric acid
k_i	Spring constant
M	Number of gold electrodes
N	Nitrogen
N	Number of gold electrodes
O	Oxygen
R	Substituent
S	Sulfur
t_i	Time

Greek letters

δ	Dirac delta function
ε_i	Strain
σ	Stress
c	Damping coefficient

Abbreviations

AFM	Atomic force microscopy
Arg	Arginine acid
Asp	Aspartic acid
BBB	Biological breadboard
CV	Cyclic voltammetry
DAPI	4’,6-Diamidino-2-Phenylindole
DMEM	Dulbecco’s modified Eagle medium
DMSO	Dimethyl sulfoxide
DOF	Degree-of-freedom
DPBS	Dulbecco’s phosphate buffered saline
ECM	Extracellular matrix
FA	Focal adhesion
FBS	Fetal bovine serum
FX	Focal complex
Gly	Glycine acid

Lys	Lysine acid
MW	Molecular weight
NIH 3T3	Mouse embryonic fibroblast cell line
PBS	Phosphate buffered saline
PEG	Polyethylene glycol
Phe	Phenylalanine acid
RGD	Arginine-glycine-aspartic acid
SAM	Self-assembled monolayer
SEM	Scanning electron microscope
XPS	X-ray photoelectron spectroscopy

DEDICATION

To my father, mother, brother, sister, and wife

CHAPTER 1. INTRODUCTION

1.1 Cellular dynamics

A cell in biology is the smallest structural and functional unit of an organism that integrates all essential life processes, the dynamics of which can provide a wealth of information concerning biological phenomena. To fully inderstand cellular dynamics *in vivo*, our bioengineers and biologists are required to carry out the following research topics: technical realization of spatiotemporal detachment at a (sub)cellular level, leading into the programmable manipulation of adherent cell motility; quantitative analysis of spatiotemporal detachment at a (sub)cellular level to characterize the expression and development of focal adhesions (FAs) during cellular detachment; measurement of viscoelastic properties of the thin layer of a living cell which is detached from a substrate and in turn retracting at a subcellular level. These cellular dynamic phenomena, especially (sub)cellular detachment from microenvironment, regulate cell function and behavior, the quantitative characterization of which will lead us to understand critical biological phenomena such as embryonic development, inflammatory immune response, wound repair, cancer metastasis, etc.[1]

The cellular dynamics has recently received considerable attention due to its important roles in biology. Even though a tremendous amount of research has revealed important information about fundamental understanding of basic cellular function and behavior (i.e., cell growth and metabolism, creation of new cell, cell movement), these extensive efforts have been limited to qualitative analyses.[2-5] A quantitative measurement of cellular dynamics has remained elusive and challenging.[6] This seems because the existing methods, previously developed for the characterization of *in vivo* cellular dynamics, has their own technical limitations. The research is designed to develop addressable, multi-functional, and reusable biological platforms, nicknamed *biological breadboards (BBBs)*, to enable the *spatiotemporal manipulation of cell motility* at cellular and even subcellular levels, offering a new method to analyze cellular dynamics in a quantitative way.

1.2 Previous methods for cellular dynamics characterization

In the cellular dynamics study, the development of a new biological platform that allows for spatiotemporal manipulation on cellular behaviors (i.e., adherent cell motility) at subcellular and cellular levels is a desperate need but a highly challenge. Previous methods developed for the study of cellular dynamics primarily focused on cell positioning or patterning, placing a cell (or confluent cells) at a target location with a designed shape, but could not spatiotemporally manipulate cell motility. The previous approaches can be classified into photolithography[7,8], e-beam lithography[9], dip-pen lithography[10], nanoimprint lithography[11], microcontact printing[12,13], ink-jet printing[14], switchable surface[15], elastomeric stencil[16], optical tweezer[17], and (di)electrophoresis.[18,19]

Although the conventional lithography technologies were used over wide applications, they generally showed several inherent drawbacks: expensive and complex facilities including a clean room were required; cell positioning was determined only at the beginning of microfabrication; once a cell was placed, it could not be modified; manipulation of adherent cell motility could not be made with the lithography

technologies. The microcontact printing method was unable to direct cell motility and to make any change in the configuration of a biological platform during experiments. The ink-jet printing method was time-consuming and also could not manipulate cell motility spatiotemporally. The switchable surface was a promising method for cell motility control but its biocompatibility was questionable. Moreover, its fabrication could be made with special facilities through complex chemical processes. The elastomeric stencil had the same problems with the microcontact printing method. The manipulation of adherent cell with the optical tweezer was impossible; it was known to make some denaturation on a living cell. The (di)electrophoresis was unable to spatiotemporally manipulate cell motility and had a possibility of cell electrolysis. As an alternative for spatiotemporal manipulation of cell motility, many researchers attempted to functionalize a substrate surface to selectively attach or detach a cell to or from the surface[15,20,21] which were yet far from directing cell motility spatiotemporally. Recently, Bhatia *et al*.[22] tried to manipulate a distance between two kinds of cells with two pieces of micromachined silicon substrates, each of which has an interlocking snap-lock mechanism. Although they controlled the distance between two different cells, this method also failed to manipulate cell motility spatiotemporally.

1.3 Biological breadboards for cellular dynamics characterization

In order to overcome the shortcomings of previous methods, new biological platforms composed of M×N identical and independently operated gold electrodes on Pyrex glass substrate, BBBs, are developed here that are able to manipulate cell motility at a (sub)cellular level by deliberately detaching a living cell or a part of the cell. The exquisite features of the platforms in cellular dynamics characterization, obtained from those of a solderless breadboard in electrical engineering, can be summarized into addressability, multifunctionality, reusability, and ease to use. The gold electrodes are designed to be independently operated so that the BBBs are entitled to addressability. Secondly, the BBBs, owing to their working principle, are multifunctional so that they can perform many spatiotemporal manipulations of cell motility such as (sub)cellular detachment, cell patterning, cell migration control, etc. This is similar to an electrical breadboard used for almost all temporary prototypes of analog and digital circuits. Thirdly, an electrochemical reaction of thiol-gold self-assembled monolayer (SAM) under negative bias potential makes the BBBs reusable. Moreover, the BBBs can be easily incorporated with other conventional instruments without any special accessory. By virtue of these features, they can offer biologists a new experimental method for exquisite manipulation of cell motility, thereby making it possible to quantitatively characterize cellular dynamics with low-effort and short-time. In the BBBs, a spatial manipulation of cell motility is achieved by activating the electrodes of interest, whereas a temporal manipulation of cell motility is accomplished by activating them at an intended time. This spatiotemporal manipulation also allows a living cell to move into a designed area by detaching a part of the cell from the BBBs.

1.4 Potential impacts of biological breadboards

For the last seven decades, a science community has made utmost efforts to understand a living cell works, which have been rewarded with qualitative data.[23] However, as time goes on, a quantitative interest in cellular dynamics has awakened. A scientific

community has been willing to understand how a cell functions in a physical and quantitative way. To some extent, the focus has been changed to the precise measurement of quantities that will help us to understand essential biological phenomena in a more exact way.[24] This situation open a door to our new biological breadboards because they allow for the programmable manipulation of adherent cell motility, and consequently yield quantitative analyses of cellular dynamics.

There are several expected impacts on scientific and non-scientific communities by our new biological platforms. The BBBs are designed to be incorporated with other conventional instruments commonly used in bioengineering and biology. With the BBB, a significant part of scientific and non-scientific communities will be beneficiated in understanding cellular dynamics. To explain how this will happen, it is worth to mention that the reusability of the BBBs make themselves cost-effective and environmentally friendly, which can also be a possible substitute to a commonly used plastic Petri dish, a major portion of biowastes and biological wastes in bioengineering and biology. The environment is therefore less harmed, which is a major concern among all of us. Also, the fact that there is not yet a well-developed biological platform for the programmable manipulation of adherent cell motility shows that the BBB can provide bioengineers and biologists with a new experimental method to characterize cellular dynamics. As an indispensible tool which will be used in many different laboratories, the BBB will help to solve scientific problems arising from cell function (i.e., machanotransduction), pathophysiology, disease progression and its theraphy, etc.[4]

1.5 Dissertation outline

Chapter 2 describes the structure and working principle of the BBBs, followed by their design and fabrication, including surface treatment in Chapter 3. Chapter 4 provides the experimental apparatus for the fabricated BBBs as well as experimental results. Finally, Chapter 5 summarizes the important scientific findings of this research.

CHAPTER 2. STRUCTURE AND WORKING PRINCIPLE

2.1 Overview

New addressable, multi-functional, and reusable biological platforms (biological breadboards or BBBs) are intended to manipulate the motility of an adherent cell at subcellular and cellular levels, thereby leading quantitative characterization of cellular dynamics. The BBBs are designed to be composed of M×N identical and independently operated gold electrodes on Pyrex glass substrate to secure the addressability in cell motility manipulation. Due to their superb working principle which will be introduced, the BBBs play critical roles (i.e., cell positioning, cell patterning, cell migration) in cellular dynamics characterization. In addition, our platforms have resuablilty originated from their electrochemistry, thereby potentially replacing a traditional biological tool, plastic Petri dish.

2.2 Structure of BBB

The BBBs consisting of identical and independently operated gold electrodes are designed to secure their addressability, achieving a high-degree-of-freedom (DOF) in spatiotemporal manipulation of cell motility, as shown in Fig. 2.1.

The spatiotemporal manipulation of cell motility is implicated by two fundamental mechanisms, cell attachment and detachment. The first mechanism is solved by a bio-inspired approach where a tri-peptide motif of arginine-glycine-aspartic acid (RGD), a recognition sequence for integrin binding to many extracellular matrix (ECM) proteins, is tethered to a gold electrode via thiol linker[25] to promote cell adhesion, as shown in Fig. 2.2*A*. A RGD-terminated thiol, thiol being chemically combined with RGD, connects a RGD peptide into the gold electrode using its one end (thiol) which shows a spontaneous chemisorption of $\text{R-S-H} + \text{Au} \rightarrow \text{R-S-Au} + 1/2\,\text{H}_2$ where R is a substituent; the other end (RGD) provides a cell-grasping site for a cell. The second mechanism depends on a rapid reductive desorption of the thiol-gold SAM under negative bias voltage. The SAM starts to be reductively desorbed with negative potential of -0.9 V, following an electrochemical reaction[26] of $\text{R-S-Au} + \text{H}^+ + \text{e}^- \rightarrow \text{R-S-H} + \text{Au}$ which makes the RGD-terminated thiol and even the cell thereon detached from the gold electrode, as shown in Fig. 2.2*B*.

2.3 Working principle of BBB

2.3.1 Bio-inspired cell adhesion mechanism

A cell in general binds to a surface or an extracellular matrix using cell adhesion molecules. An integrin, one of the most common transmembrane proteins, is known as a receptor that mediates an attachment between cell and microenvironment which may be other cell or ECM with cell attachment site (e.g. RGD). A RGD peptide that serves as a cell adhesion motif constitutes a major recognition system for cell adhesion together with the integrin[27,28], as shown in Fig. 2.3*A*. The integrin-mediated attachment needs to be kept intact or similar to that of *in vivo* because it regulates critical cellular function and behavior such as cell migration, growth, differentiation, and apoptosis. The RGD peptide was therefore invited to provide a cell with a microenvironment which is biologically

identical with *in vivo* one, thereby achieving a cell adhesion mechanism in the BBBs. A RGD-terminated thiol, borrowed from biology, was used in a surface-treatment for: chemical binding of the RGD peptide into a gold electrode through spontaneous chemisorption of thiol with gold; giving a cell adhesion site to a living cell with RGD peptide, as shown in Fig. 2.3*B*. This surface-treatment plays important roles in the spatiotemporal manipulation of cell motility: adhering a living cell to a surface through RGD peptide; detaching the cell from the substrate through the rapid reductive desorption of a gold-thiol SAM under negative potential.

2.3.2 Cell detachment mechanism

In the BBBs where a living cell binds to the RGD-terminated thiol and stretches on a substrate before activation, (sub)cellular detachment from the substrate depends on a rapid reductive desorption of the thiol-gold SAM under negative bias voltage. The SAM starts to be reductively desorbed with negative potential of -0.9 V, according to $\mathrm{R\text{-}S\text{-}Au} + \mathrm{H^+} + \mathrm{e^-} \rightarrow \mathrm{R\text{-}S\text{-}H} + \mathrm{Au}$. This electrochemical reaction makes the RGD-terminated thiol detached from the gold electrode. Thus, a cell or parts of the cell placed on the activated gold electrode is detached and then contracting because all adherent cells are under tension.

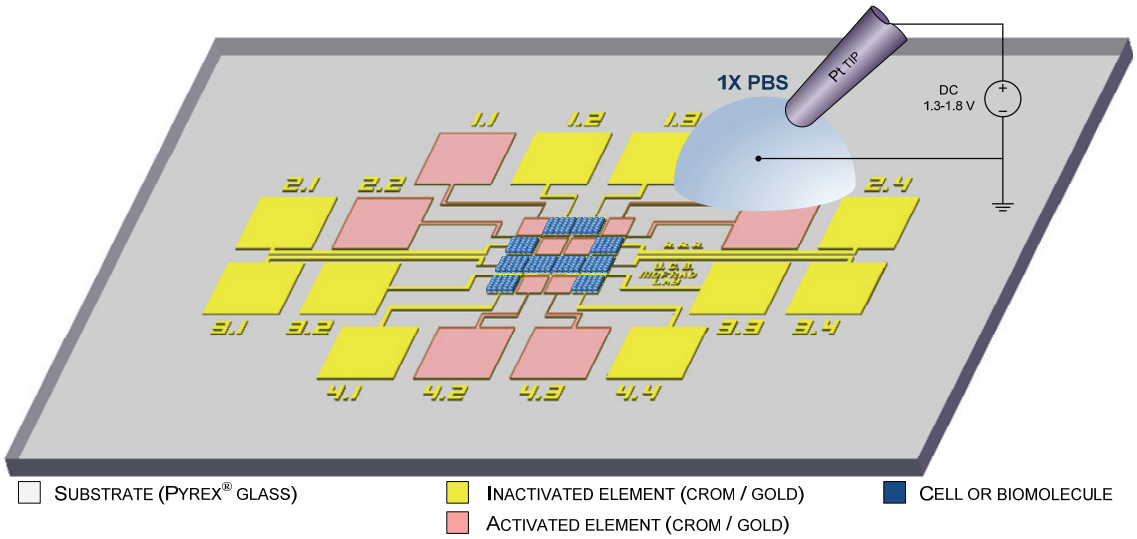

Figure 2.1 Biological breadboards (BBBs) for subcellular manipulation and characterization. Schematic of the BBBs consisting of M×N gold electrodes placed on a Pyrex glass. The addressability, multifunctionality, and reusability of the BBBs are derived from their exquisite structure and working principle (electrochemistry).

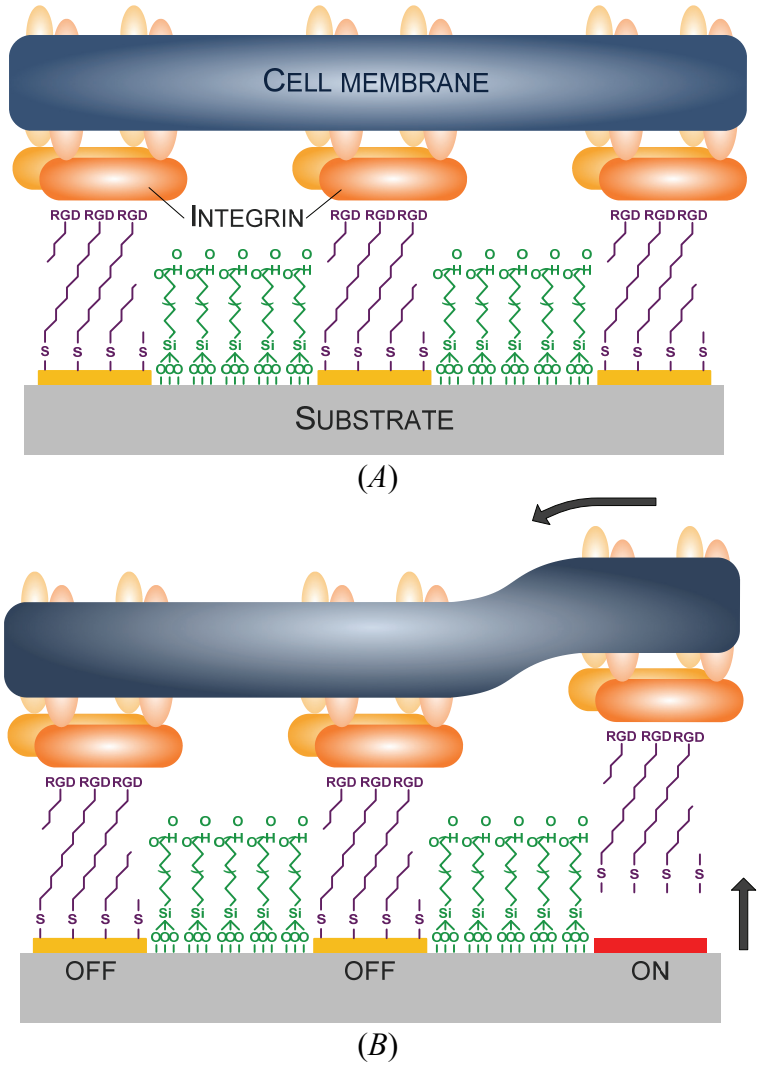

Figure 2.2 Working principle of the BBBs. (*A*) Before (sub)cellular detachment, a RGD-ligand binding to integrin, focal contact, is formed on a gold electrode treated with RGD-terminated thiol (cell-adhesive surface), whereas no focal contact is formed on a Pyrex glass treated with PEG (cell-resistive surface). (*B*) Upon (sub)cellular detachment with low bias potential, a living cell or parts of the cell binding to the RGD-ligand is detached and then spontaneously contracting.

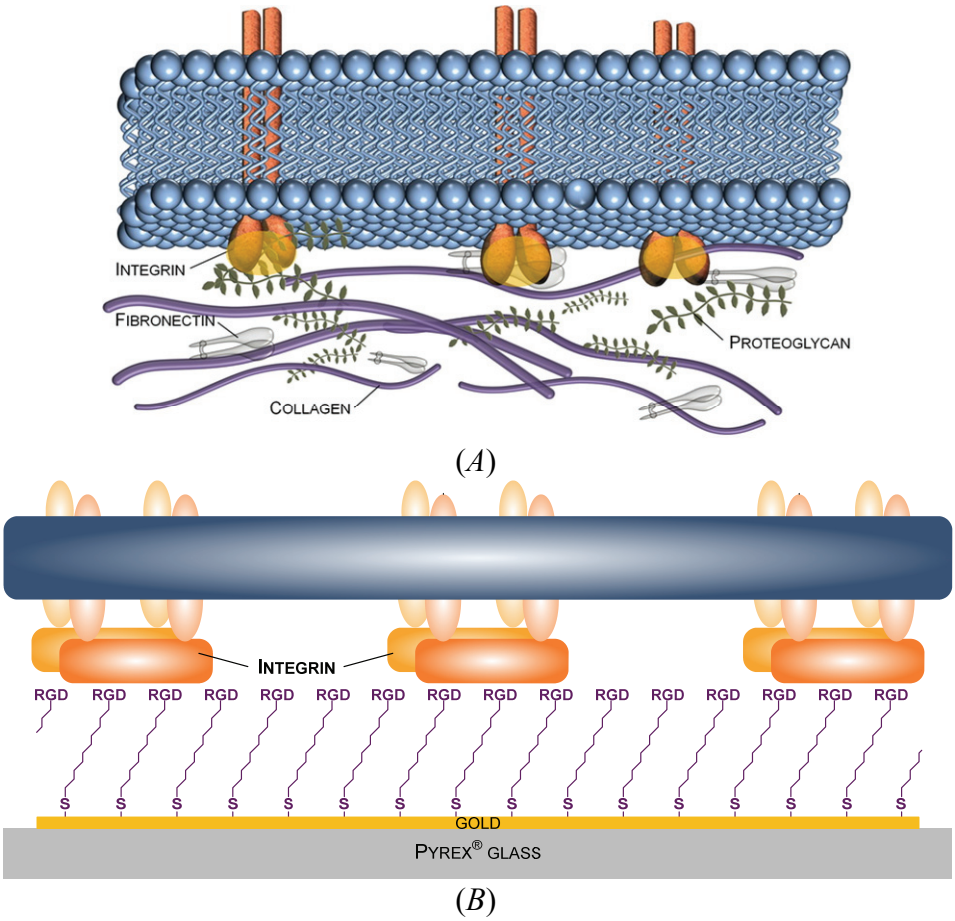

Figure 2.3 Bio-inspired cell adhesion mechanism of the BBBs. (*A*) A living cell adheres to a substrate through the cellular interaction of a transmembrane protein, integrin, with an extracellular matrix protein, RGD, in nature. (*B*) A living cell is tethered to a gold electrode via RGD-terminated thiol in the BBBs.

CHAPTER 3. DESIGN AND FABRICATION

3.1 Microfabrication processes

Microfabrication processes combining optical lithography, e-beam evaporation, and lift-off processes were used to fabricate two different types of the BBBs, one for cellular detachment whose gold electrode is 500 μm in length and 500 μm in width, and one for subcellular detachment whose gold line is 10 μm in width and 3 μm in its neighboring gap. The detailed microfabrication processes of the BBBs are as follows.

The BBBs were microfabricated on a 4-inch Pyrex glass wafer with a thickness of 500 μm (University Wafer). After its cleaning with a piranha solution of 1:1 (v:v) 96% sulfuric acid (H_2SO_4) and 30% hydrogen peroxide (H_2O_2) for 10 minutes, 1 μm-thick LOR resist (LOR 10A, MicroChem Corp.) was spin-coated at 4000 rpm for 40 seconds, followed by soft baking at 170˚C for 5 minutes. A 2 μm-thick positive photoresist (S1818, Rohm and Haas Corp.) was spin-coated on the LOR resist at 4000 rpm for 40 seconds for double-layer resist stack, followed by soft baking at 110˚C for 1 minute. An optical lithography was done to pattern the double-layer resist stack before an e-beam evaporation process, as shown in Fig. 3.1*A*. The next was a deposition of 5 nm-thick chromium (Cr) adhesion layer and 100 nm-thick gold (Au) layer on the wafer, as shown in Fig. 3.1*B*. As a color transparency in the visual spectrum is essential to make the BBBs incorporated with other biological instrument (e.g. inverted optical or fluorescent microscopes), the Au layer thickness was reduced to be 30 nm for biological experiments, as shown in Fig. 3.2, *right*. After the deposition of Cr and Au layers, this wafer was immersed in an organic solvent mixture (BAKER PRS-3000 Stripper, Mallinckrodt Baker, Inc.) at 80˚C for 4 hours to lift off the double-layer resist stack, as shown in Fig. 3.1*C*.

The fabricated BBBs were wire-bonded in a chip carrier, followed by assembling them with a cell-culture-wall made of acrylic resin. The microfabricated BBBs is shown in Fig. 3.2 where the left is a device after wire bonding in a chip carrier and assembling with a cell-culture-wall, and the right is a device before them. The left and right insets in Fig. 3.2 are the scanning electron microscope (SEM) images of the BBBs for cellular detachment (*left inset*) and subcellular detachment (*right inset*).

3.2 Surface-treatment processes

The surfaces of the fabricated BBBs were modified by two surface-treatments, as shown in Fig. 3.3: polyethylene glycol (PEG) treatment on Pyrex glass and RGD-terminated thiol treatment on gold. The first is intended to achieve a “cell-resistive” surface which suppresses cell spreading on it. This prevents a cell from adhering on Pyrex glass, which makes it easy to spatiotemporally manipulate cell motility with (sub)cellular detachment. The second is planned to tether a RGD peptide into gold via thiol linker, thereby providing a “cell-adhesive” surface.

The PEG treatment was accomplished by incubating the BBBs in 2% v/v PEG silane and 1% v/v hydrochloric acid dissolved in anhydrous toluene for 2 hours at room temperature. This reaction was carried out in a glove box under a nitrogen purge to prevent the PEG silane from being exposed to atmospheric moisture. For RGD-terminated thiol treatment, a RGD-terminated thiol solution was synthesized by combining *cyclo* (Arg-Gly-Asp-D-Phe-Lys) ($C_{27}H_{41}N_9O_7$, MW 603.68) with succinimide-terminated thiol, followed by immersing the BBBs into the solution for 2 hours at room

temperature. This surface-treatment was also done in a moisture-free environment. The detailed surface-treatment processes of the BBBs are as follows.

3.2.1 Surface-treatment of Pyrex glass with polyethylene glycol

Considering the main functions of the BBBs, their Pyrex surface without gold needs to be cell-resistive. The surface coated with PEG is known to show anti-fouling behavior owing to steric repulsion between hydrated neutral PEG chain and protein.[29,30] Moreover, the PEG-modified surface is anti-cell adhesive and consequently suppresses cell spreading even a focal contact on the surface because a cell-adhesion mechanism is protein-mediated.[31,32] After microfabrication, the Pyrex glass surface of the BBBs was modified with PEG as follows. The BBBs were treated in an oxygen plasma chamber (PM-100 Plasma Treatment System, March Plasma Systems, Inc.) at 100 W for 30 seconds. The BBBs were then incubated in 2% v/v PEG silane and 1% v/v hydrochloric acid (Fisher Scientific) dissolved in anhydrous toluene (Fisher Scientific) for 2 hours. This reaction was carried out in a glove box under a nitrogen purge to avoid atmospheric moisture. After this surface-treatment, the BBBs were rinsed in fresh toluene and ethanol, dried under nitrogen, and cured at 120°C for 2 hours. The modified BBBs were stored in a vacuum desiccator until the next surface-treatment, RGD-terminated thiol treatment. The PEG is coated only on the Pyrex glass surface because Pyrex glass has hydroxyl groups on its surface but gold surface does not, as shown in Fig. 3.4*A*.

3.2.2 Surface-treatment of gold with arg-gly-asp-terminated thiol

The gold electrodes of the BBBs need to be cell-adhesive in order to promote the adhesion of adherent cell into the surfaces. For this purpose, the gold electrodes of the BBBs were treated with RGD-terminated thiol whose solution was synthesized by chemically combining a *cyclo* (Arg-Gly-Asp-D-Phe-Lys) ($C_{27}H_{41}N_9O_7$, MW 603.68, Peptides International, Inc.) with dithiobis(succinimidyl undecanoate) ($C_{30}H_{48}N_2O_8S_2$, MW 603.68, Dojindo Molecular Technologies, Inc.) as follows. The *cyclo* (Arg-Gly-Asp-D-Phe-Lys), *c*(RGDfK), was dissolved in dimethoxysulfoxide (DMSO, Sigma-Aldrich) to get 1 mM aliquot and stored at -20°C. This reaction was made in a glove box under a nitrogen purge to prevent the *c*(RGDfK) from being exposed to atmospheric moisture. The maximum storage period for this solution was 15 days because the peptide easily loses its characteristics (e.g. anchor for $\alpha_v\beta_3$ integrin). The dithiobis(succinimidyl undecanoate) was also stored in 1 mM aliquot in DMSO at -20°C. This preparation was also done in a moisture-free environment. Before the gold surface-treatment, both aliquots were warmed to room temperature in a desiccator. The *c*(RGDfK) aliquot was mixed with triethylamine (1% v/v, Fisher Scientific) for 5 minutes to make all primary amines of the lysine amino acid unprotonated. The same volume of the dithiobis(succinimidyl undecanoate) was added to the *c*(RGDfK) aliquot and then mixed well using a vortex mixer for 4 hours to synthesize the RGD-terminated thiol solution. During the gold surface-treatment, the microfabricated BBBs were incubated with the solution for 1 hour at room temperature to promote a spontaneous chemisorption between thiol and gold, followed by sonificating them in DMSO for 3 minutes, rinsing them in ethanol and phosphate buffered saline (PBS, Sigma-Aldrich) to eliminate all unbound RGD-terminated thiol from the gold surface. The thiol contacted with gold made a SAM

according to $\text{R-S-H} + \text{Au} \rightarrow \text{R-S-Au} + 1/2\text{H}_2$, thereby tethering RGD peptide to gold element, as shown in Fig. 3.4*B*.

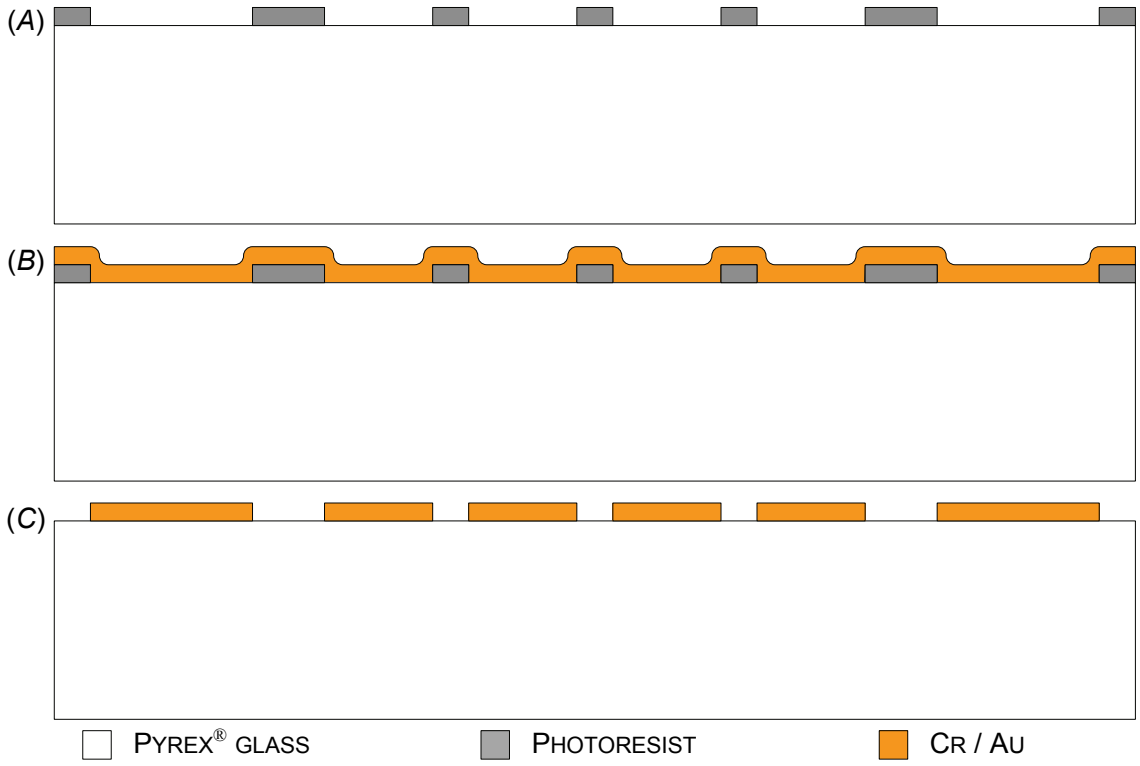

Figure 3.1 Microfabrication processes of the BBBs. (*A*) Patterning of photoresist by lithography. (*B*) Deposition of chrome and gold layers by e-beam evaporation. (*C*) Patterning of the deposited Cr/Au layer by lift-off.

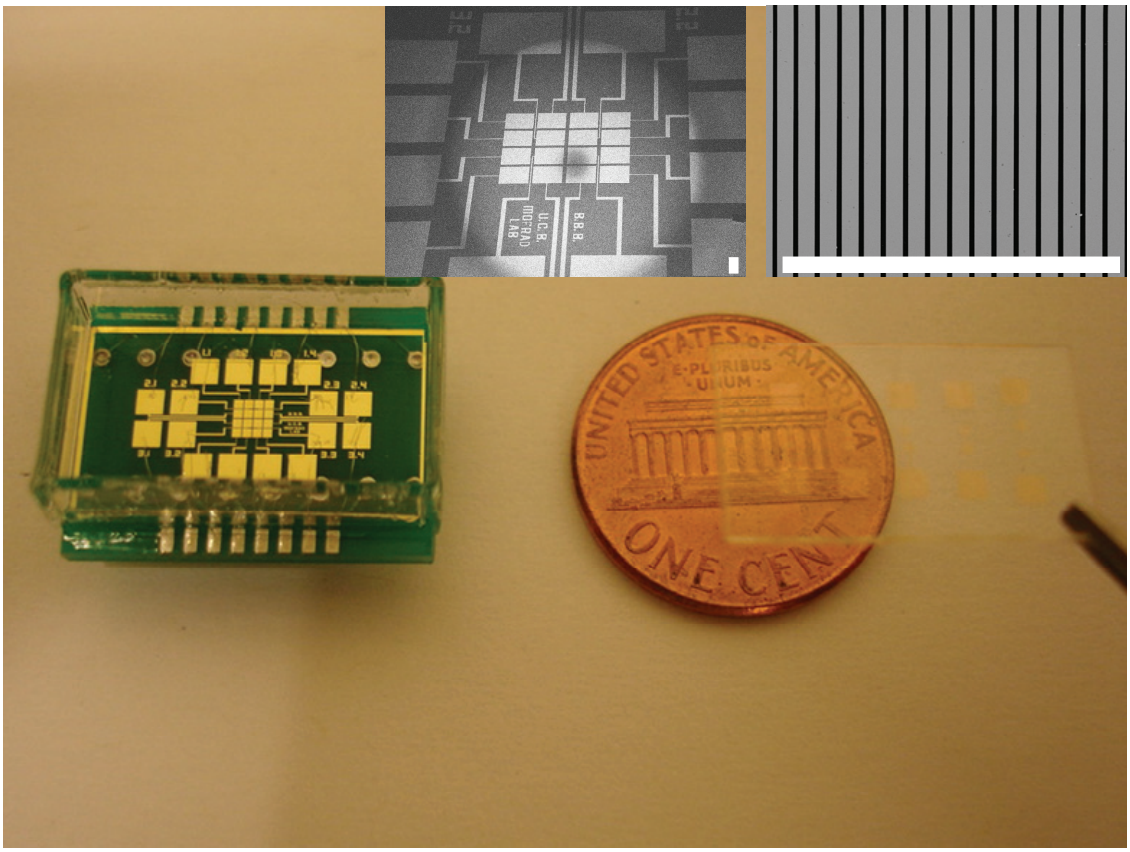

Figure 3.2 Photograph of the BBBs after (*left*) and before (*right*) assembly, showing its transparency in the visual spectrum. The BBBs for cellular detachment and subcellular detachment are shown in left and right insets, respectively. Scale bar is 100 μm.

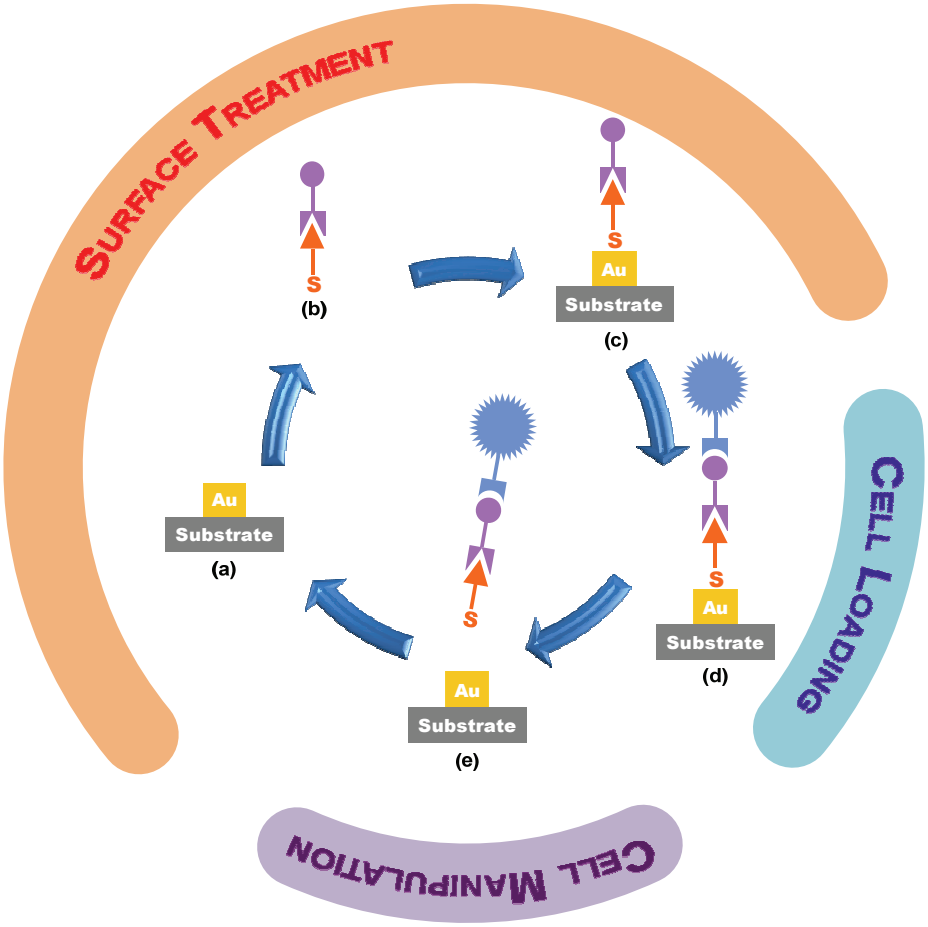

Figure 3.3 Surface-treatment processes of the BBBs. Microfabricated BBBs (*a*) are incubating with a PEG solution to achieve a cell-resistive surface on a Pyrex glass surface, followed by incubating them with a synthesized solution of RGD-terminated thiol (*b*) to achieve a cell-adhesive surface on a gold electrode (*c*). After loading a living cell on the BBBs (*d*), a cell or a part of the cell is detached with low bias potential (*e*).

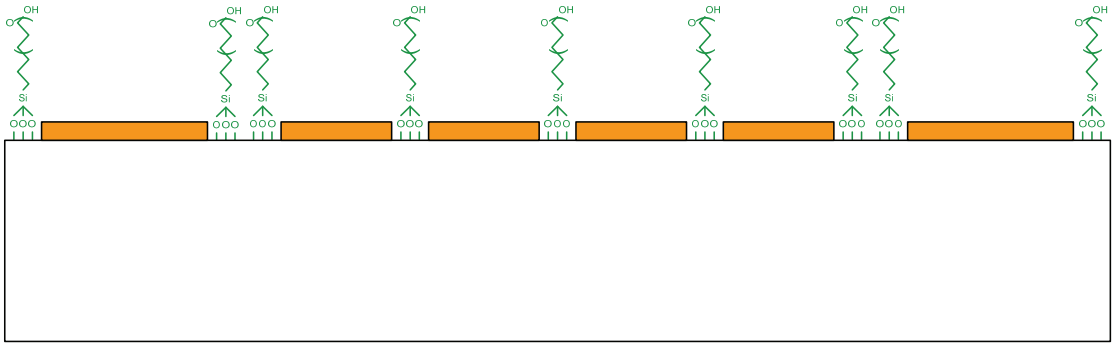

(*A*)

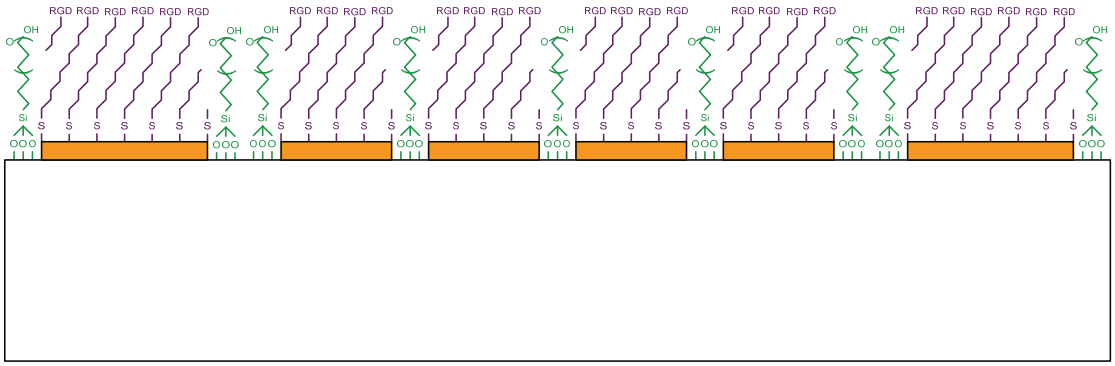

(*B*)

Figure 3.4 Detail surface-treatment processes of the BBBs. (*A*) PEG treatment on Pyrex glass surface to achieve a "cell-resistive" surface. (*B*) RGD-terminated thiol treatment on gold surface to chemically tether the RGD peptide into the gold electrodes.

CHAPTER 4. EXPERIMENTAL CHARACTERIZATIONS

4.1 Surface-treatment characterization

The quality of the surface-treatment was investigated both by measuring a contact angle using a goniometer and by detecting the atoms in the treated surface using an x-ray photoelectron spectroscopy (XPS) system.

4.1.1 Characterization of surface-treatment by contact angle measurement

Two surface-treatments using PEG and RGD-terminated thiol were made to achieve cell-resistive and cell-adhesive surfaces, respectively. To characterize the surface-treatment quality, a contact angle on the modified surface was measured by a goniometer. A contact angle measurement system (KRÜSS582, KRÜSS) was used to measure the contact angle in a sessile drop mode which is usually used to estimate the wetting properties of a solid surface. Based on 10 time measurements, the contact angle of the PEG treated Pyrex glass surface was 61.5±3.8˚ whereas that of the untreated Pyrex glass surface was 25.7±1.5˚, as shown in Fig. 4.1*A*, *upper*. This indicates that the PEG treated surface has a strong hydrophobicity, and consequently prevents a cell adhesion or protein fouling. A cell loading test using NIH 3T3 cell (mouse embryonic fibroblast cell line) was also made, as shown in Fig. 4.1*A*, *lower*. The images obtained after 24 hours of cell loading show the Pyrex glass surface has been modified into cell-resistive.

To characterize the RGD-terminated thiol treatment, a contact angle was measured for bare gold, gold with thiol only, and gold with RGD-terminated thiol. The averaged contact angles of them were 67.3±2.5°, 53.3±1.3°, and 24.6±2.8°, respectively, as shown in Fig. 4.1*B*, indicating that the RGD-terminated thiol treatment has been made as intended. These experimental results verify in an indirect way that our surface-treatments are effective to achieve the cell-resistive and cell-adhesive surfaces in the BBBs.

4.1.2 X-ray photoemission spectroscopy characterization of gold surface-treated with RGD-terminated thiol

The formation of thiol-gold SAM and the existence of RGD by RGD-terminated thiol surface-treatment were verified by an XPS survey which is a direct characterization method. An XPS sample was prepared on a 4-inch silicon wafer e-beam evaporated with 50 nm-thick Au layer and 5 nm-thick Cr adhesion layer. For the RGD-terminated thiol surface-treatment, the wafer was immersed for 2 hours in the RGD-terminated thiol solution prepared as summarized in Chapter 3. A bare gold sample without RGD-terminated thiol treatment was run as a control experiment. The XPS analysis was carried out with a customized ESCA (Omicron NanoTechnology). The measurement was performed at 1×10^{-8} Torr and all spectra referenced to the position of the Au 4f peaks. Scans were collected over a range of 20 eV around the peak of interest with a pass energy of 23.5 eV. Figure 4.2 shows the measured XPS survey spectrum of RGD/thiol/Au interface. The peaks of Au 4*s*, Au 4*p*, Au 4*d*, and Au 4*f* indicate the presence of the e-beam evaporated gold, Au(111); the peaks of S $2p_{1/2}$ and S $2p_{3/2}$ (*inset*, *right*) show the sulfur from the thiol is in existence on the surface; the peaks of C 1*s*, O 1*s*, O *KLL*, and N 1*s* (*inset*, *left*) demonstrate there are carbon, oxygen, and nitrogen from amine functional group ($-NH_2$) and carboxylic acid functional group (-COOH) of the RGD peptide, which

means the RGD peptide is connected to the surface. For reference, hydrogen cannot be detected due to the working mechanism of XPS. This XPS survey spectrum verifies that the surface-treatment using RGD-terminated thiol on the gold element has been done as designed.

4.2 Potentiodynamic electrochemical characterization of reductive desorption of thiol-gold self-assembled monolayer

A rapid reductive desorption of the thiol-gold SAM was characterized in a potentiodynamic electrochemical way – cyclic voltammetry (CV) which is the most effective electroanalytical technique in the redox system study. A voltage supplied by a constant DC power source (B&K Precision Corporation) was applied between thiol-gold SAM (or Ag/AgCl electrode) and platinum electrode. A CV sample was prepared by the same surface-treatment described in Chapter 3. The surface-treated gold element with RGD-terminated thiol was used as a working electrode while the platinum electrode and an Ag/AgCl electrode were used as a counter electrode and a reference one, respectively. The CV was carried out in the Dubecco's phosphate buffered saline (DPBS (pH 7.4), Sigma-Aldrich) solution with an EG&G potentiostat model 362 (AMETEK Princeton Applied Research). A scan started cathodically from 0 V, then annodically back to 0 V after reaching -2 V at a scan rate of 50 mV s^{-1}, as shown in Fig. 4.3*A*. The CV (Fig. 4.3*B*) shows the measured current at the working electrode as a function of the applied voltage with respect to the Ag/AgCl electrode. At a potential range of 0 V to -0.9 V (section *a*), the measured current was negligible, which means there is no reductive desorption of the SAM and consequently the SAM impedes electron transfer across an electrolyte-electrode interface. The reductive desorption of the SAM, which started and finished at a potential of -0.9 V (point *b*) and -1.55 V (point *d*) respectively, broke the chemical binding between thiol and gold at a potential range of -0.9 V to -1.55 V (section *c*). The reductive desorption of the SAM got maximize at a peak of -1.4 V. The measured CV shows an indisputable evidence of the reductive desorption of the SAM, and also demonstrates the bias potential required for (sub)cellular detachment.

4.3 Minimum size of gold electrode for cell adhesion

It is very important to make a cell adhere to the gold surface-treated with the RGD-terminated thiol for subcellular manipulation of cell motility. Twenty types of gold arrays consisting of equilateral triangular, square, regular pentagonal, regular hexagonal, or circular electrodes with an area of 64 μm^2, 100 μm^2, 225 μm^2, or 400 μm^2 were prepared to characterize the effect of the geometry and size of the gold electrode on cell adhesion. NIH 3T3 cells with a concentration of about 1×10^6 cells/ml were loaded on the surface-treated gold electrode arrays and their optical images were obtained after 24 hours of cell loading, as shown in Fig. 4.4. No cell adhered to the gold element with a side less than 10 μm (Fig. 4.4*A*), while cells made a stable adhesion to the gold element with a side larger than 10 μm (Figs. 4.4*B-D*). This is because the floated NIH 3T3 cell before cell adhesion is almost spherical and 10 μm in diameter. For the gold electrodes with the same area (or side length), the number of cells adhered to the gold electrode gets decreased as the number of side of the electrode gets increased. In other words, the equilateral triangle-shaped gold electrode is the most effective in making a cell adhesion thereon. This tendency is because equilateral triangle, assuming the same area, has the largest

circumference and a cell prefers a circumferential part of the gold element to center part for cell adhesion. For reference, the circumferences of equilateral triangle, square, regular pentagon, regular hexagon, and circle are respectively $4.56a^{1/2}$, $4a^{1/2}$, $3.81a^{1/2}$, $3.72a^{1/2}$, and $3.54a^{1/2}$ where a is an area.

4.4 (Sub)cellular detachments

4.4.1 Cell culture

NIH 3T3 mouse embryonic fibroblast cell (Instructional Lab, University of California, Berkeley) was cultured in Dulbecco's modified Eagle medium (DMEM, GIBCO™) supplemented with 10% fetal bovine serum (FBS, GIBCO™) and 1% Penicillin-Streptomycin (GIBCO™) at 37˚C in a humidified 5% CO_2 atmosphere. The cell was passaged every three days as follows. The cell was washed 1 time in PBS and trypsinized with Trypsin-EDTA solution 0.5% (1X). After centrifuging, the cell is inoculated into new Petri dish. The NIH 3T3 cell with a passage number of 5 to 20 was used in the experiment. Before experiment, the surface-treated BBB was sterilized with 70% ethanol, washed twice with 1× PBS, and placed into a Petri dish containing 5 ml of cell suspension in cell culture medium with a concentration of about 1×10^6 cells/ml. For the subcellular detachment, the cell-loading concentration was 1×10^4 cells/ml. After 1 hour, unattached NIH 3T3 cells were removed by aspirating and washing the BBB in PBS, followed by replacing old cell culture medium with new one. All experiments were carried out after 24 hours of cell loading in a self-designed chamber with a humidified 5% CO_2 atmosphere and at 37˚C.

4.4.2 Cellular detachment

The cellular detachment – detaching all parts of a living cell from substrate – of NIH 3T3 cells was made with the fabricated BBBs both to characterize cell detachment behaviors and to investigate the addressability and reusability of the BBBs, thereby evaluating the BBBs as biological platforms for spatiotemporal cell patterning or positioning. The cellular detachment experiments were carried out for three cases of single or two cells (Fig. 4.5*A*), sparse cells with about 25% confluence (Fig. 4.5*B*); confluent cells with 100% confluence (Fig. 4.5*C*). A cell-detaching time defined as a time required to detaching 95% of loaded cells was obtained from experimental results. The cell-detaching times for three cases, averaged from at least 10 time measurements at activation potential of -1.5 V, were respectively 45.2±6.8 seconds, 36.7±8.7 seconds, and 21.1±3.5 seconds, showing that more confluent cells are detached in a shorter time. This is because the detachment of confluent cells is influenced by neighboring cells. In other words, when one cell is detached, neighboring cells to the detached one is easily detached because all cells are connected to each other by a cell-to-cell interaction. To characterize the effect of activation potential on cellular detachment, a cell-detachment ratio was measured as a function of activation time and potential. A cell-detachment ratio gets decreased as activation potential gets increased, as shown in Fig. 4.6. This can be explained by the reductive desorption of thiol-gold SAM which gets faster as negative potential gets increased, as shown in Fig. 4.3*B*. The obtained cell-detachment ratio has S-shape which is monotonically increasing with two inflection points. This clearly demonstrates that there

is a large deviation in integrin binding to ECM or other cells which is closely related to a cell-to-cell interaction.

4.4.3 Selective cell patterning

Two different types of BBB platforms, composed of 2×1 and 4×4 gold electrodes respectively, were used for selective cell patterning of NIH 3T3 cells, thereby demonstrating the addressability and reusability of the BBBs in cell manipulation. The first cell patterning was made with 2×1 BBB where a left electrode was activated to detach the cells but a right one was inactivated. Figure 4.7 shows optical and immunofluorescent images where NIH 3T3 cells were stained for actins with rhodamine phalloidin (red) and for cell nuclei with DAPI (blue).

The detailed staining processes for immunofluorescence microscopy are as follows. NIH 3T3 cells grown on the BBB were stained for immunofluorescence microscopy. After fixing the cells on ice with 4% formaldehyde (Fisher Scientific) solution in chilled PBS for 15 minutes, the cells were washed 3 times with chilled PBS. The cells were permeabilized with 200 μl 0.5% Triton X-100 (Sigma-Aldrich) in PBS at room temperature for 10 minutes and were washed 3 times with PBS to make small holes in their cellular membrane, followed by blocking non-specific binding using 3% non-fat dry milk in PBS at 4˚C for 1 hour and washing the cells once with PBS. 10 μl methanolic stock solution of rhodamine phalloidin (Biotium, Inc.) was diluted with 200 μl PBS with 1% Bovine Serum Albumin (BSA, Fisher Scientific) for each BBB. The BBB was incubated with this solution for 20 minutes at room temperature and washed 2 or 3 times with PBS. For nucleus staining, ProLong® gold antifade reagent with DAPI (Invitrogen) was added into the cells. Immunofluorescent images were obtained on the inverted fluorescent microscope (Axiovert 200, Carl Zeiss MicroImaging, Inc.).

The second experiment was a selective cell patterning into “C,” “A,” and “L” shapes with a single 4×4 BBB (Fig. 4.8). This cell patterning was done in an order of “L,” “A,” and “C” by using a single device which was reused through simplified organic cleaning process after each usage. Since the reductive desorption of thiol-gold SAM yields original gold again, the BBBs can be reused. These experimental results shown above verify the exquisite addressability and reusability of the BBBs.

The detailed cleaning processes to secure the reusability of the BBBs are as follows. The reductive desorption of a thiol-gold SAM according to $\mathrm{R\text{-}S\text{-}Au} + \mathrm{H^+} + \mathrm{e^-} \rightarrow \mathrm{R\text{-}S\text{-}H} + \mathrm{Au}$ yields bare gold again, entitling reusability to the BBBs. Thus, the BBBs are cost-effective and environment-friendly. The BBBs were cleaned to reuse them after each use in the following method. After each use, all cells on the BBBs were detached with negative potential of -1.5 V, followed by adding Trypsin-EDTA solution 0.5% (1X) (Sigma-Aldrich) to completely remove all cellular materials known as integrin remnants;[33] the remnants were also eliminated by sonificating the BBBs with acetone for 8 minutes, rinsing it 3 times with ethanol (Fisher Scientific), rinsing them 3 times with ethanol (Fisher Scientific), and rinsing them again 7 times with deionized water. The cleaned BBBs were inspected with an optical microscope to check their surface. Although one or two remnants were occasionally left on the cleaned BBBs (Fig. 4.9, *circle*), there was no problem in reusing them. This indicates that our cleaning process described above is enough to secure their reusability. Because of their reusability,

the BBBs are expected to contribute in reducing a use of disposable experimental stuff in biological experiments, thereby solving a major concern among all of us, environment protection.

4.4.4 Viability characterization of detached cell

In our BBBs, the spatiotemporal manipulation of cell motility is done by deliberately detaching a living cell at a (sub)cellular level. A detached cell should be therefore alive rather than electrocuted after (sub)cellular detachment. If a detached cell from the BBBs is electrocuted, these platforms cannot perform their functions as biological platforms for (sub)cellular manipulation and characterization. Thus, this characterization was made to bring forward a clear-cut evidence showing that a detached cell is still alive, that is, viability of detached cell. In this experiment, NIH 3T3 cells bound to the BBBs were detached by an electrical activation signal of -1.5 V, followed by collecting the detached cells with a centrifuge and loading them into a plastic Petri dish. After 24 hours of cell loading, their viability was observed, as shown in Fig. 4.10. This observation shows that about 75% of the detached cells are still alive after cellular detachment. Compared to a general cell passage at which about 95% of cells are viable, this result is comparable and lays a technical foundation for spatiotemporal manipulation of cell motility by (sub)cellular detachment of a living cell with the BBBs.

4.4.5 Subcellular detachment

Single cell motility was manipulated by subcellular detachment with the BBB consisting of 10 μm-width gold electrode lines with a gap of 3 μm (Fig. 3.2, *right inset*). At subcellular detachment, RGD peptides are linked to all gold electrodes except activated ones. Since a living cell in general has much higher affinity for RGD peptide than for gold surface, a cell exposed to subcellular detachment is subject to spontaneously move into a designated direction. For example, when some part of a cell (cytoplasm) located at 3 o'clock direction is detached, the cell migrates into 9 o'clock direction. The subcellular detachment experiment was performed to open a possibility for spatiotemporal manipulation of cell motility and also to show the multifunctionality of the BBBs, i.e. cell patterning and cell motility control. A subcellular detachment experiment using NIH 3T3 cell was made with the same experimental conditions and apparatus as those of cellular detachment. As shown in the optical sequential images of the subcellular detachment (Fig. 4.11), the subcellular detachment was accomplished by contracting a detached cytoplasm which reaches its completion within 16 seconds. This relative fast contraction of subcellular detachment using a single cell, compared to that of cellular contraction using confluent cells, can be explained by high-strain state of a cell. A single cell is always under higher-strain than confluent cells are because there is no constraint in stretching itself with focal contacts, thereby leading a fast contraction of the detached cytoplasm in the subcellular detachment.

In the next subcellular detachment experiment, a cell was sequentially detached with a series of activations where the first activation (activation 1) was followed by the second one (activation 2) after 16 seconds. The optical sequential images (Fig. 4.12) reveal that repetitive activations within dozens of seconds do not have any influence on cell's viability and a subcellular-detaching amount is gradually increasing.

4.5 Measurement of viscoelastic properties in the detached and retracting thin cytoskeletal layer of fibroblasts

4.5.1 Overview

The thin layer of mouse fibroblast NIH 3T3 cells, detached from a substrate and in turn retracting, is investigated to characterize its viscoelastic properties using time-sequential image of the thin layer retraction in conjunction with atomic force microscopy indentation on it. The former is intended to acquire the normalized-strain profile of the retracting motion of a thin layer, while the latter is made to determine its elastic strength. The measured viscoelastic properties have demonstrated that the detached and retracting thin layer of fibroblasts has 67% decreases in elastic strength but 30-fold increases in damping capacity, compared to an attached one.

A living cell reversely polymerizes soluble actin monomers into filaments by incorporating the monomers with accessory proteins at its thin layer, leading or trailing edge. This biological phenomenon is believed to provide the cell with main motile force for migration by extending (or detaching) and attaching (or retracting) a thin layer. Any irregularity in the cell's physical properties may therefore undermine the biological functions of the cell in health and disease, potentially leading to serious pathophysiological consequences of mental retardation, vascular disease, tumor formation, etc.[34] The physical properties, e.g. viscoelasticity, of the thin layer therefore must be quantitatively characterized for a better understanding of cellular dynamics.

There have been a variety of methods developed to measure the physical properties of a cell, which can be classified into a magnetic-particle-based cytometry,[35] a micropipette aspiration,[36] an optical tweezer,[37] a fluid shear flow method,[38] a cytoindenter,[39] and an atomic force microscopy (AFM).[40] These approaches are, however, mostly limited to adherent cells with no motion and cannot help in quantification of the physical properties of the motile thin layer (less than 1 μm). In this experiment, the viscoelastic properties of the motile thin cytoskeletal layer of fibroblasts are measured by incorporating the retraction profile of the detached thin layer from a substrate with the elastic modulus measured by AFM indentation, thereby yielding a continuum mechanical model for the motile thin cytoskeletal layer.

4.5.2 Viscoelastic model of detached and retracting thin cytoskeletal layer

When a cell repeatedly extends a leading edge, translocating a nucleus, detaching (retracting) a trailing edge during its life cycle, the strain versus time diagram of a thin layer can be simplified, as shown in Fig. 4.13*A*. A thin layer extends and attaches to a substrate at $0 \le t < t_1$; it translocates a nucleus with keeping its morphology at $t_1 \le t < t_2$; it is detached and in turn is retracting at $t_2 \le t$. A standard linear viscoelastic solid model composed of two springs k_1, k_2 and one dashpot c (Fig. 4.13*B*) is adopted to describe the retraction motion of the detached thin layer, and consequently to quantify its dynamic viscoelastic properties. Assuming that the thin layer is isotropic and viscoelastic, this model is used because it can take two phenomena of creep and stress relaxation into account.

Assuming that the thin layer is an isotropic and viscoelastic continuum, its stress σ and stress ε are written as

$$\sigma = k_1\varepsilon_1 = k_2\varepsilon_2 + c\dot{\varepsilon}_2, \tag{4-1}$$

$$\varepsilon = \varepsilon_1 + \varepsilon_2, \tag{4-2}$$

where the subscripts of 1 and 2 refer to the springs of elastic and viscous components, respectively. Combining these two equations yields

$$(k_1 + k_2)\sigma + c\dot{\sigma} = k_1k_2\varepsilon + k_1c\dot{\varepsilon}. \tag{4-3}$$

A unit-cell migration mechanism enables us to assume the stress and strain profiles of the thin layer at the STEP-I ($0 \le t < t_2$, relaxation phase) as follows. The initial stress at $t = t_1$ is σ_0 and the strain is a Heaviside function with a jump of ε_0 at $t = t_1 \approx 0$ due to $t_1 \ll t_2$,

$$\begin{aligned} \varepsilon(t) &= \varepsilon_0 H(t), \\ \dot{\varepsilon}(t) &= \varepsilon_0 \delta(t), \end{aligned} \tag{4-4}$$

where $H(t)$ is a Heaviside function and $\delta(t)$ is a Dirac delta function. The linear viscoelastic equation about stress and strain can be rewritten as

$$(k_1 + k_2)\sigma(t) + c\dot{\sigma}(t) = k_1k_2\varepsilon_0 H(t) + k_1c\varepsilon_0\delta(t). \tag{4-5}$$

The Laplace transformation of above equation yields

$$\sigma(t) = \frac{k_1k_2}{k_1 + k_2}\varepsilon_0\left(1 - e^{-\frac{k_1+k_2}{c}t}\right) + \sigma_0 e^{-\frac{k_1+k_2}{c}t}. \tag{4-6}$$

The stress σ_{t2} of the thin layer at $t = t_2 \approx \infty$ is therefore expressed as

$$\sigma_{t2} = \frac{k_1k_2}{k_1 + k_2}\varepsilon_0. \tag{4-7}$$

At the STEP-II ($t \ge t_2$, creep phase) where the strain exponentially decays from ε_0 to zero after the thin layer is detached at $t = t_2$, the stress is considered as an inverted Heaviside function with a jump of σ_{t2} at $t = t_2$,

$$\begin{aligned} \sigma(t) &= \sigma_{t2}\left(1 - H(t - t_2)\right), \\ \dot{\sigma}(t) &= -\sigma_{t2}\delta(t - t_2). \end{aligned} \tag{4-8}$$

Using these two equations, the viscoelastic equation about stress and strain is represented as

$$(k_1 + k_2)\sigma_{t2}\left(1 - H(t - t_2)\right) - c\sigma_{t2}\delta(t - t_2) = k_1 k_2 \varepsilon(t - t_2) + k_1 c\dot{\varepsilon}(t - t_2). \quad (4\text{-}9)$$

The stain profile at the STEP-II is calculated through the Laplace transformation of above equation,

$$\varepsilon(t - t_2) = \varepsilon_0 \left(1 - \frac{k_2}{k_1 + k_2}\right) e^{-\frac{k_2}{c}(t - t_2)}. \quad (4\text{-}10)$$

Thus, the strain profile normalized with respect to ε_0 is therefore given by

$$\varepsilon^* = \frac{\varepsilon(t - t_2)}{\varepsilon_0} = \left(1 - \frac{k_2}{k_1 + k_2}\right) e^{-\frac{k_2}{c}(t - t_2)}. \quad (4\text{-}11)$$

4.5.3 Image acruisition of detached and retracting thin cytoskeletal layer

For the image acquisition of the retraction motion of a detached thin layer, the BBBs (Fig. 3.2, *right insect*) composed of multiple gold electrodes on Pyrex substrate were fabricated the microfabrication techniques of optical lithography, e-beam evaporation, and lift-off process. Each gold electrode, 10 μm in width and 3 μm in neighboring gap, was functionalized with a RGD-terminated thiol to achieve a cell-adhesive surface, whereas the Pyrex substrate was coated with the a PEG to provide a cell-resistive surface which suppresses cell spreading on it. One end (RGD peptide) of the RGD-terminated thiol constitutes a major recognition system for cell adhesion and the other end (thiol compound) connects the RGD peptide into the gold electrodes by making a gold-thiol self-assembled monolayer (SAM) following the spontaneous chemisorption of $\text{R-S-H+Au} \rightarrow \text{R-S-Au+1/2}\,\text{H}_2$ where R is a substituent. Before subcellular detachment (Fig. 2.2*A*), a cell binds to the RGD peptide through its integrin and stretches on the surface of the biological platform. Upon subcellular detachment (Fig. 2.2*B*), the thin layer of a cell is detached by a rapid reductive desorption of the SAM under low bias voltage of -1.3 to -1.8 V, $\text{R-S-Au+H}^+\text{+e}^- \rightarrow \text{R-S-H+Au}$. Based on this electrochemical reaction, the RGD-terminated thiol and even the thin layer thereon can be detached from the gold electrodes.

A subcellular detachment experiment using fibroblast was performed with the fabricated biological platform dipped in the CO_2 independent media containing 10% FBS and 1% pen-strep at 36˚C. An electrical activation signal was given by a three-electrode system composed of a gold (of the BBB), a platinum, and an Ag/AgCl electrodes which play as working, counter, and reference electrodes, respectively. The retraction behavior of the detached thin layer was recorded with a charge-coupled device camera. A strain profile of the detached thin layer was obtained from the recorded time-sequential images (Fig. 4.11); being normalized with respect to initial strain ε_0 (Fig. 4.14); being fitted into

an exponential curve using a commercial data analysis software (Origin Pro 8, Exp2PMod1 mode). Through this curve fitting, a mathematical function that has the best fit to the experimental results was determined as $\varepsilon^* = 0.799e^{-0.055t}$ showing $k_1/(k_1+k_2) = 0.799$ and $k_2/c = 0.055$.

4.5.4 AFM indentation

As these two equations were not enough for calculating the three parameters of k_1, k_2, and c, the elastic modulus of the detached thin layer of fibroblasts was measured with an Autoprobe CP AFM (Park Science Instruments) at a low-speed of 10 nm/s which can quantify an elastic modulus without involving viscous damping. The elastic modulus was obtained by these slow indentations on the detached thin layer by measuring the deflection of an AFM microcantilever at each point of interest.

The detailed AFM indentation method is as follows. The elastic modulus of the detached thin layer of fibroblast cells was measured with an Autoprobe CP AFM. All measurements were made at a low-indentation-speed of 10 nm/s to eliminate a viscous damping effect, by the dashpot of the detached thin layer, in quantifying the elastic modulus. The elastic modulus was determined by measuring the deflection of an AFM microcantilever (HYDRA2R-100N, Nanoscience Instruments, Inc.) at each point of interest of the fibroblasts. Although the AFM microcantilever has a nominal spring constant of 0.011 N/m, the measured spring constant of the AFM microcantilever was determined as 0.016±0.005 N/m, which was used in the AFM indentation in this experiment. Before AFM indentations (Fig. 4.15), the furthermost end of the thin layer of fibroblasts (indicated by "○" in the inset of Fig. 4.16) was lightly held with a glass microcapillary (TransferTip-RP, Eppendorf) to prevent a spontaneous retraction of the thin layer after subcellular detachment. With the subcellular detachment but no retraction motion, the AFM indentations were made at the thin layer (indicated by "+" in the inset of Fig. 4.16). All indentations were carried out for fibroblasts, after 24 hours of cell loading, in the CO_2 independent media with 10% FBS and 1% pen-strep at a chamber whose temperature is maintained at 36˚C with a thermal heater.

The measured cantilever deflection as a function of base displacement for the detached thin layer (Fig. 4.16) shows the elastic modulus ($k_{\text{total}} = k_1 k_2/(k_1+k_2)$) is about 1320±310 Pa, averaged value from 10 measurements. By combining the normalized-strain profile with the AFM indentation results, k_1, k_2, and c of the thin layer of fibroblasts, detached and retracting, were determined as 6567 Pa, 1652 Pa, and 30037 Pa·sec, respectively. Compared to the previous results[40, 41] of $k_{\text{total}} > 4000$ Pa and $c < 100$ Pa·sec obtained not from the thin layer of a fibroblast cell with motion but from adherent cell without motion, the detached and retracting thin cytoskeletal layer showed 67% decreases in elastic modulus and a 30-fold increase in damping coefficient. This suggests that the retracting thin layer gets softer, and consequently has remarkable increase in damping coefficient after a few seconds of detachment when subject to no physical constraint, i.e. no focal contact. This phenomenon is likely owing to the gel-sol transition of short actin filaments at subcellular detachment which leads to the changes in the viscoelastic properties of the motile thin layer of fibroblasts. When a cross-linked network of short actin filaments that are strongly coupled to focal contacts gets depolymerized upon subcellular detachment, the structural strength of the thin layer is decreasing but the

viscous damping capacity is increasing. In conclusion, the viscoelastic properties in the motile thin layer of mouse fibroblast NIH 3T3 cells after subcellular detachment have been investigated in an experimental method. The measured results have demonstrated that the method combining the time-sequential images of subcellular retraction with AFM indentation results is ideally suited for measuring the viscoelastic properties of the motile thin layer, thereby leading to a better understanding of cellular dynamics.

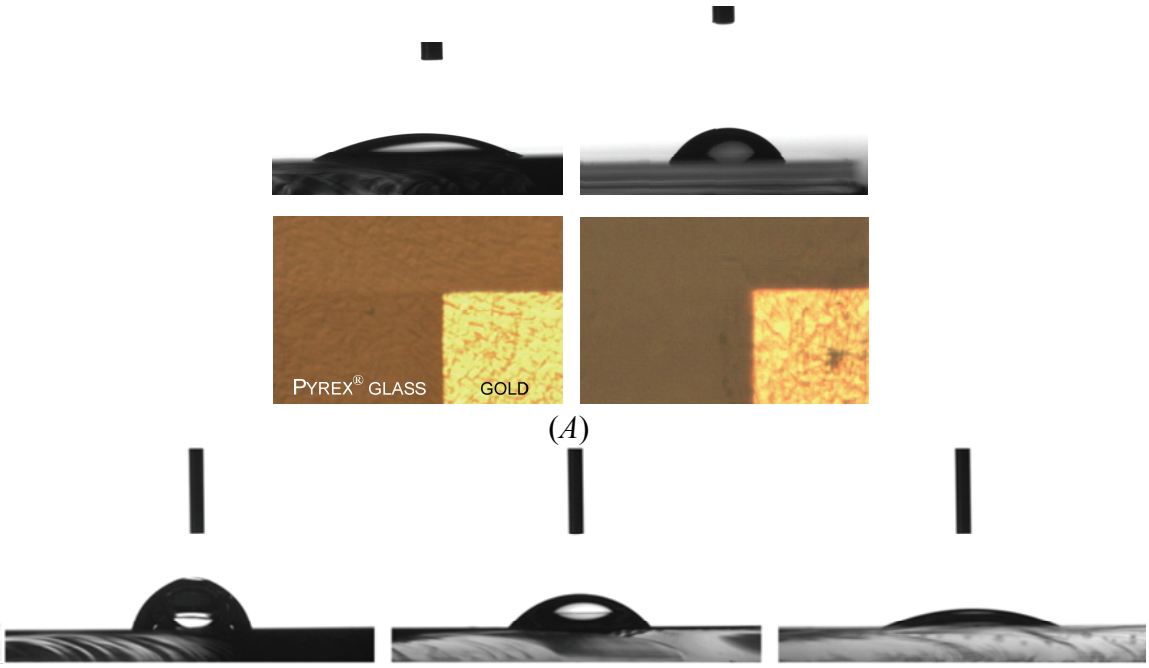

(*A*)

(*B*)

Figure 4.1 Characterizations of two surface-treatments. (*A*) Measured contact angle of the Pyrex glass before (*upper left*) and after (*upper right*) PEG treatment. Cell culture on the Pyrex glass before (*lower left*) and after (*lower right*) PEG treatment, showing the non-fouling effect of PEG treatment on the Pyrex glass surface. (*B*) Measured contact angle of gold surface without surface-treatment (*left*), with thiol treatment (*middle*), and with RGD-terminated thiol treatment (*right*), showing a surface modification by RGD-terminated thiol treatment.

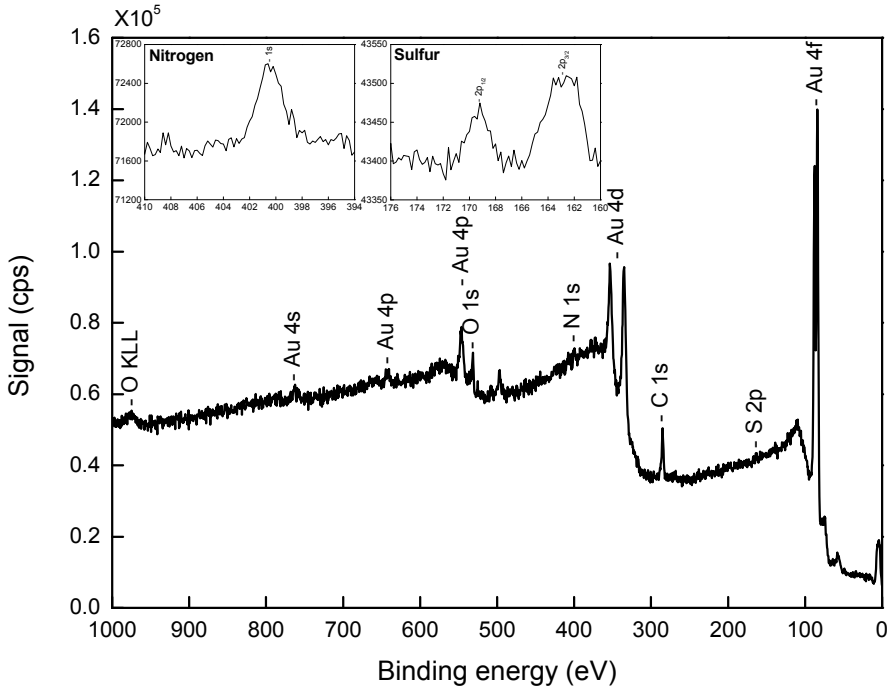

Figure 4.2 X-ray photoelectron spectroscopy survey spectrum of the gold surface-treated with RGD-terminated thiol, showing that gold peak from gold element, sulfur peak from thiol, nitrogen peak from amine group of RGD peptide, carbon and oxygen peaks from carboxylic acid group of RGD peptide are existed in the treated gold surface.

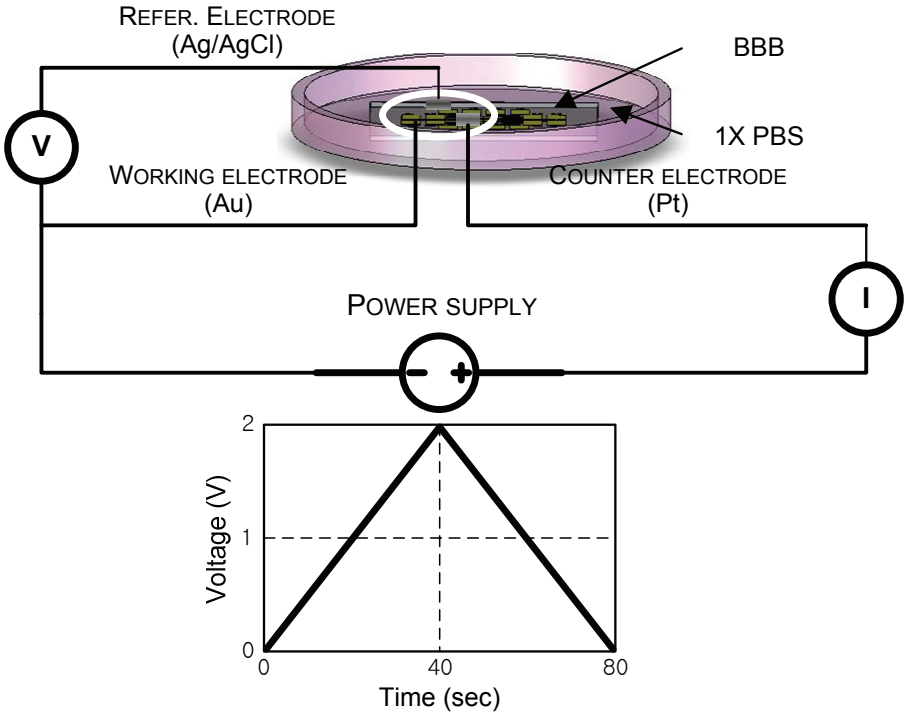

(*A*)

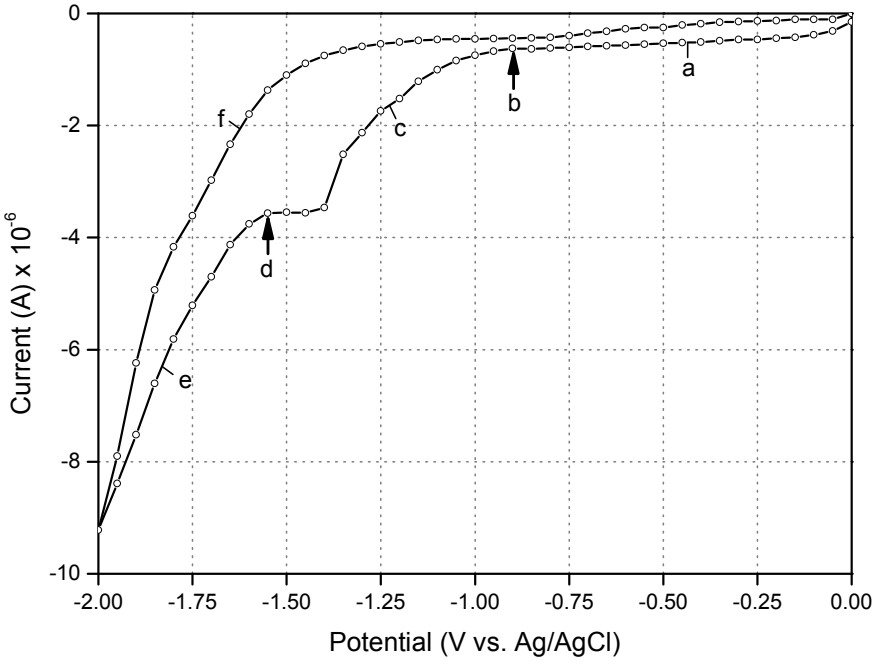

(*B*)

Figure 4.3 Electrochemical characterization of reductive desorption of thiol-gold self-assembled monolayer. (*A*) Experimental setup for potentiodynamic electrochemical characterization of the thiol-gold SAM composed of three electrodes and a power supply.

(*B*) Cyclic voltammogram, showing a reductive desorption of the thiol-gold SAM.

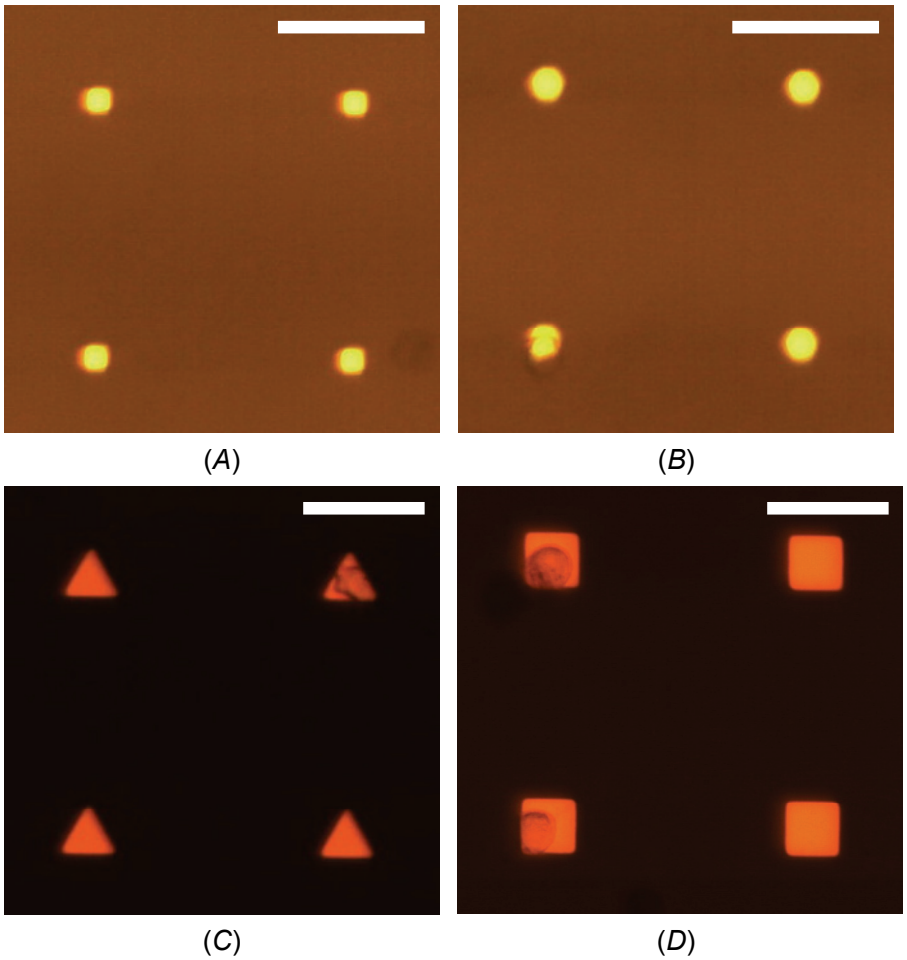

Figure 4.4 Various gold elements with different shape and size. (*A*) 64 μm^2-sized square gold electrodes. Cell adhesion is on none of them. (*B*) 100 μm^2-sized regular hexagonal gold elements. Cell adhesions are on about 25% of them. (*C*) 225 μm^2-sized equilateral triangular gold elements. Cell adhesions are on about 25% of them. (*D*) 400 μm^2-sized square gold elements. Cell adhesions are on about 50% of them. Scale bars are 50 μm.

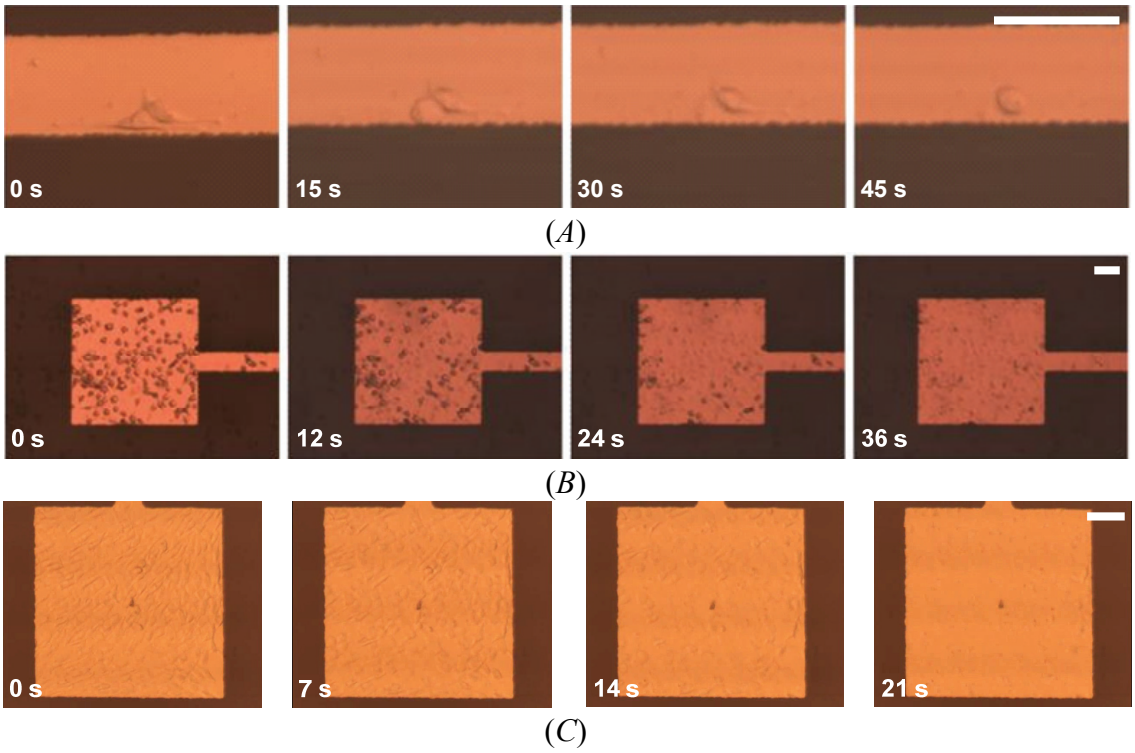

Figure 4.5 Cellular detachment (or patterning) of NIH 3T3 cell using the BBBs. (*A*) Optical sequential images, showing a cellular detachment of two cells from a gold electrode. The average cell-detaching time for single or two cells is 45.2±6.8 seconds. (*B*) Cellular detachment of cells with 25% confluence whose average cell-detaching time is 36.7±8.7 seconds. (*C*) Cellular detachment of cells with 100% confluence whose average cell-detaching time is 21.1±3.5 seconds. Scale bars are 100 μm.

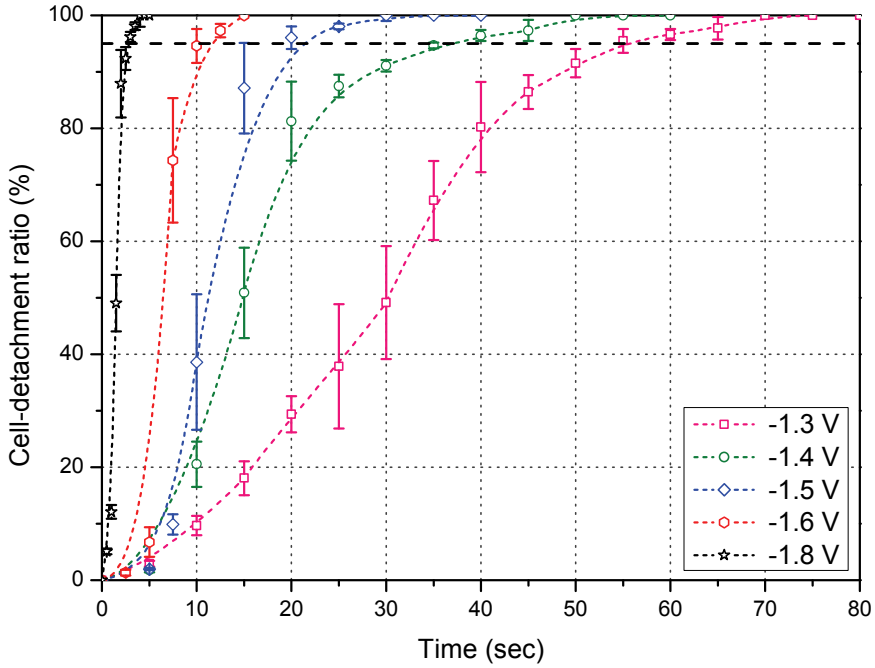

Figure 4.6 Measured cell-detachment ratio as a function of activation time and potential for 100% confluent cells. This cell-detachment ratio is S-shaped, indicating that there is a large deviation in integrin binding to ECM or other cells which is directly related to a cell-to-cell interaction.

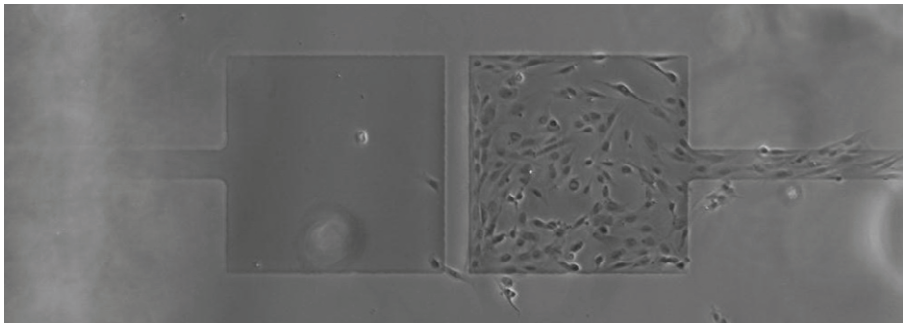

(*A*)

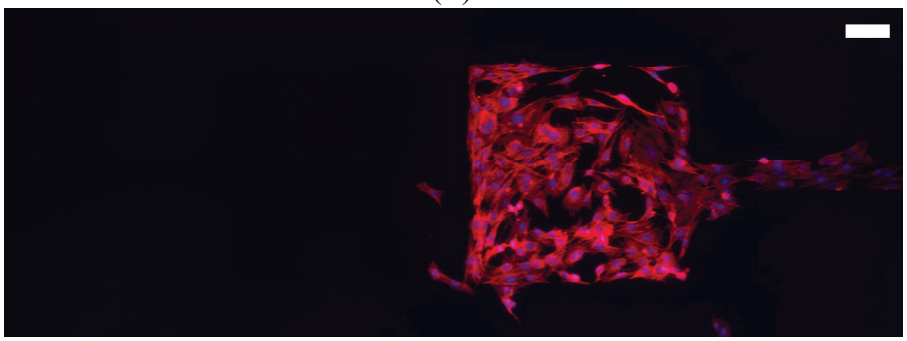

(*B*)

Figure 4.7 Selective cell patterning using the BBBs. (*A*) Optical image. (*B*) Immunofluorescent image. These show that the selective cell patterning of a 2×1 BBB where left electrode is activated but right one is inactivated. For this immunofluorescent imaging, NIH 3T3 cells were stained for actin with rhodamine phalloidin (red) and for cell nucleus with DAPI (blue). Scale bar is 100 μm.

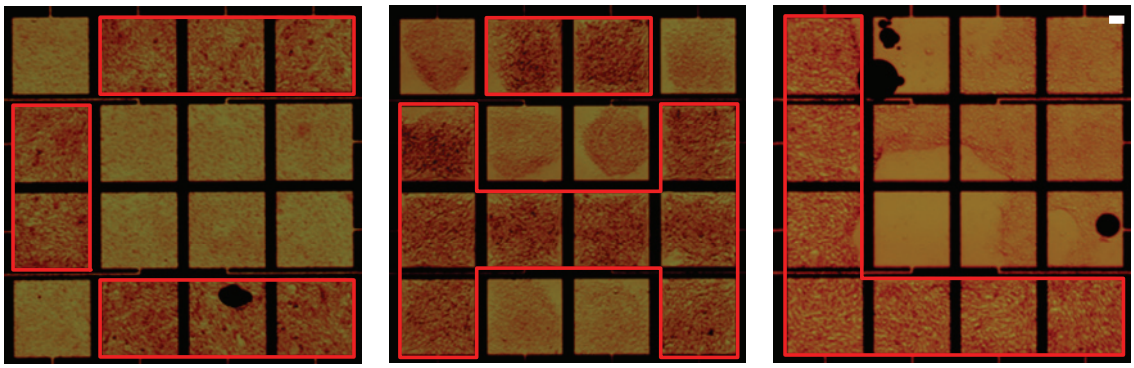

Figure 4.8 Cell patterning into “C,” “A,” and “L” shapes using a single 4×4 BBB, verifying its addressability and reusability. Scale bar is 100 μm.

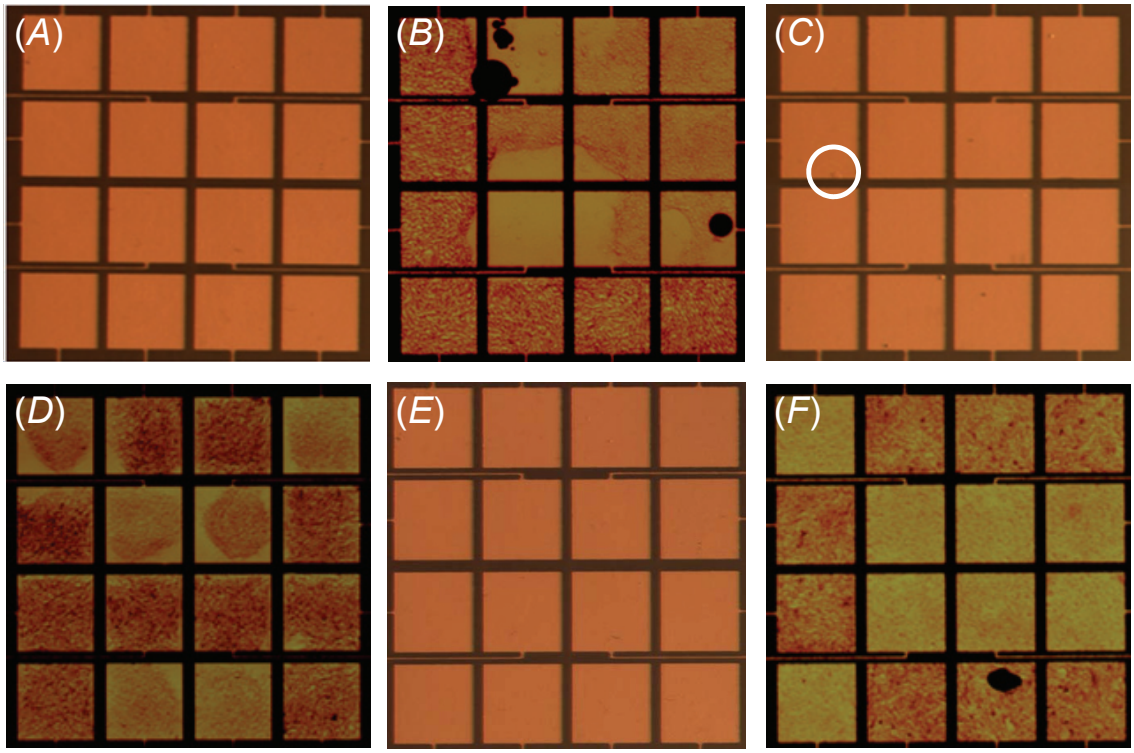

Figure 4.9 Reusability characterization of the BBBs. (*A*) Unused BBB. (*B*) First use of the BBB. (*C*) First cleaning of the BBB. (*D*) Second use of the BBB. (*E*) Second cleaning of the BBB. (*F*) Third use of the BBB.

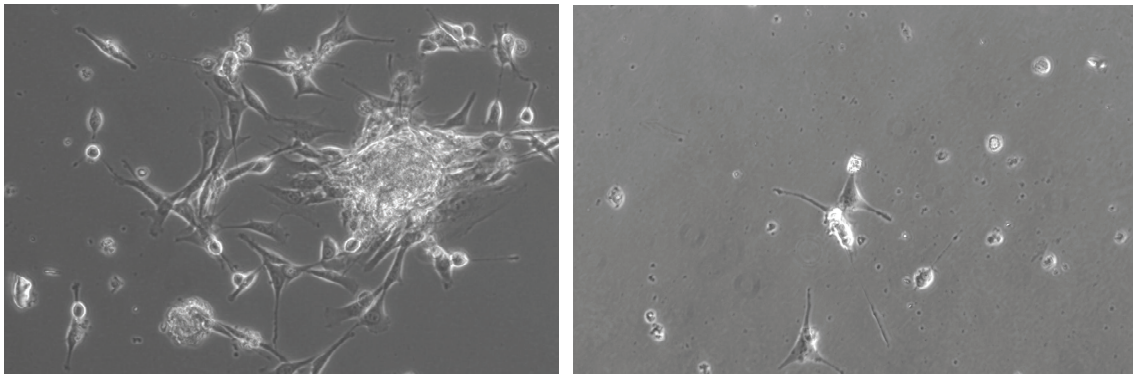

Figure 4.10 Cell viability characterization after (sub)cellular detachment.

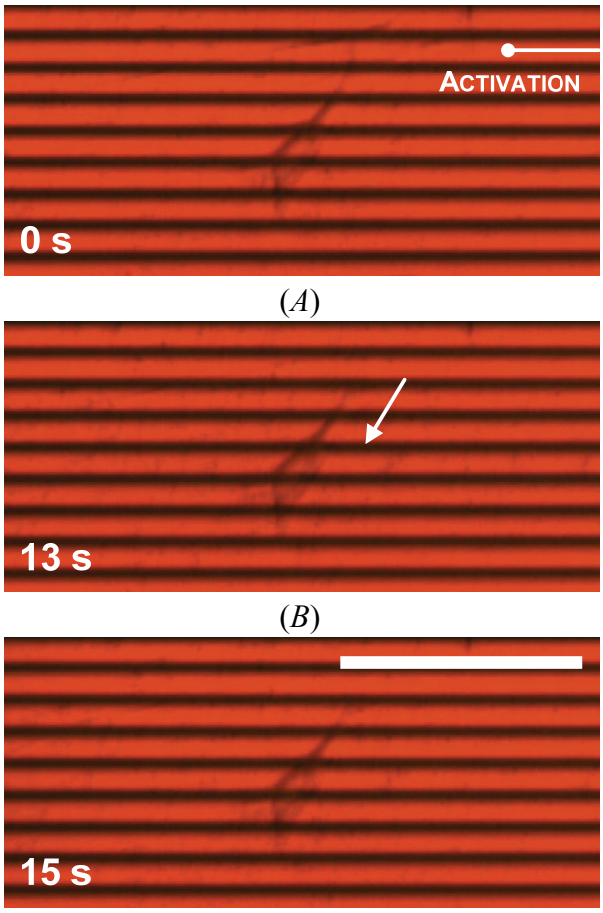

Figure 4.11 Subcellular detachment of a NIH 3T3 cell with single activation. (*A*) 0 secone. (*B*) 13 seconds. (*C*) 15 seconds. This subcellular detachment is accompanied by spontaneous contraction of a detached part of the cell.

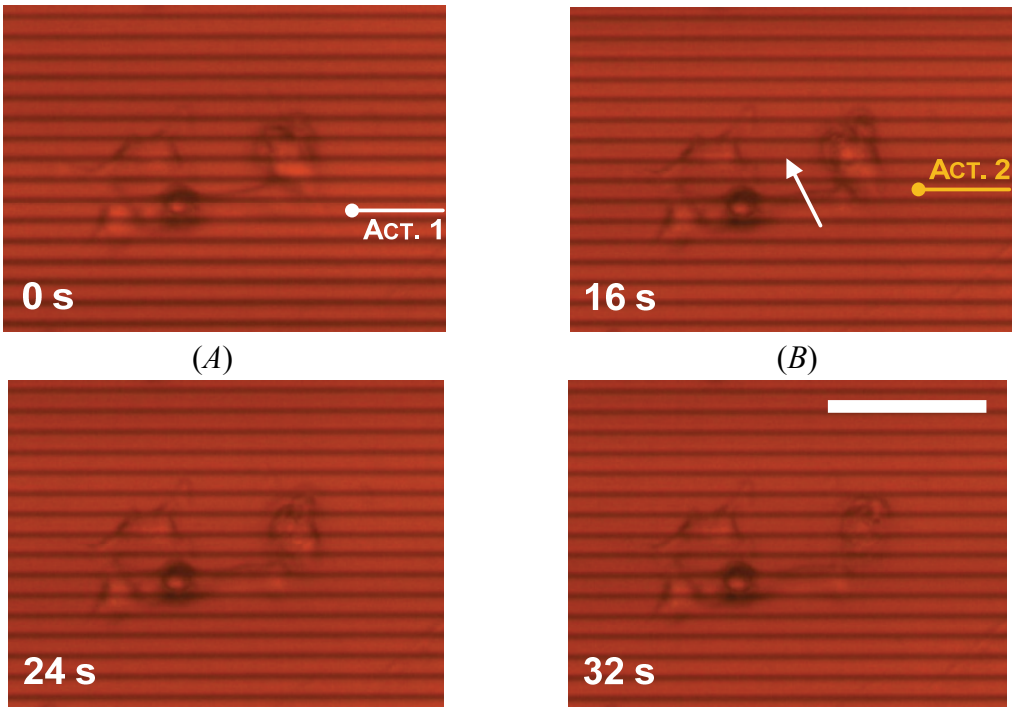

Figure 4.12 Subcellular detachment with a series of activations. (*A*) 0 secone. (*B*) 16 seconds. (*C*) 24 seconds. (*D*) 32 seconds.

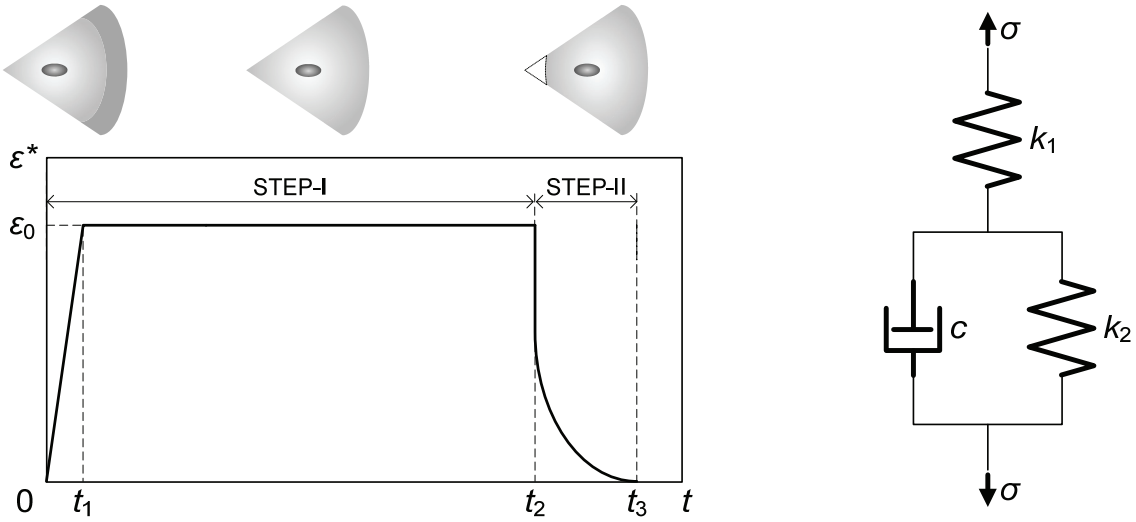

Figure 4.13 A cell behavior during its life cycle. (a) Strain-time diagram of a living cell: being loaded to a substrate ($t = 0$); extending a protrusion at its front edge ($0 < t < t_1$); translocating its nucleus ($t_1 \le t < t_2$); being detached and retracting at a subcellular level ($t_2 \le t$). (b) Continuum mechanical model for the detached and retracting thin layer of a cell.

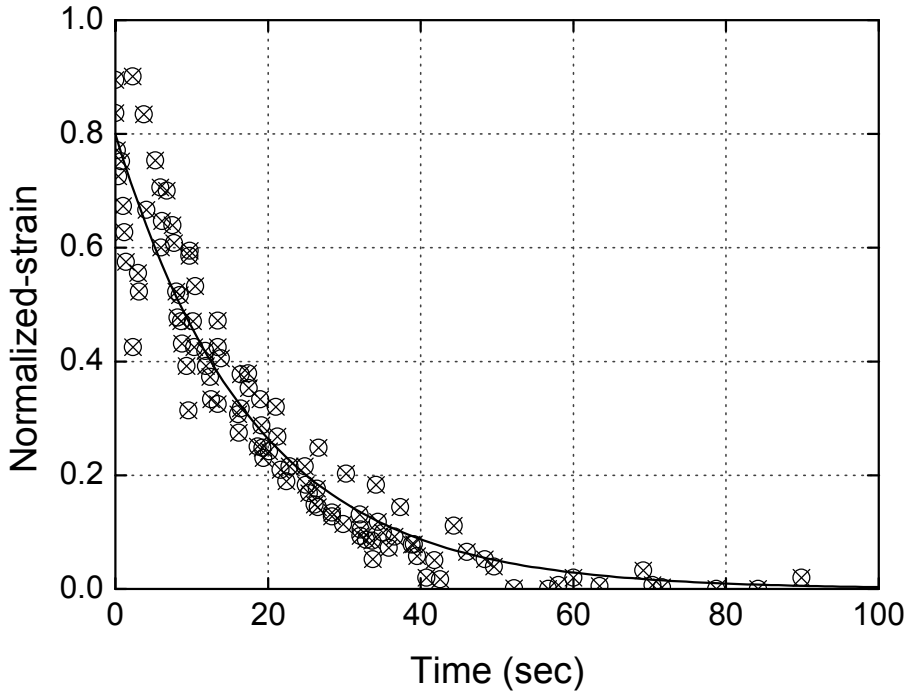

Figure 4.14 Subcellular detachment and retraction using the biological platform. Measured normalized-strain ε^* as a function of time t of fibroblasts detached in a subcellular level, which is fitted into $\varepsilon^* = 0.799e^{-0.055t}$.

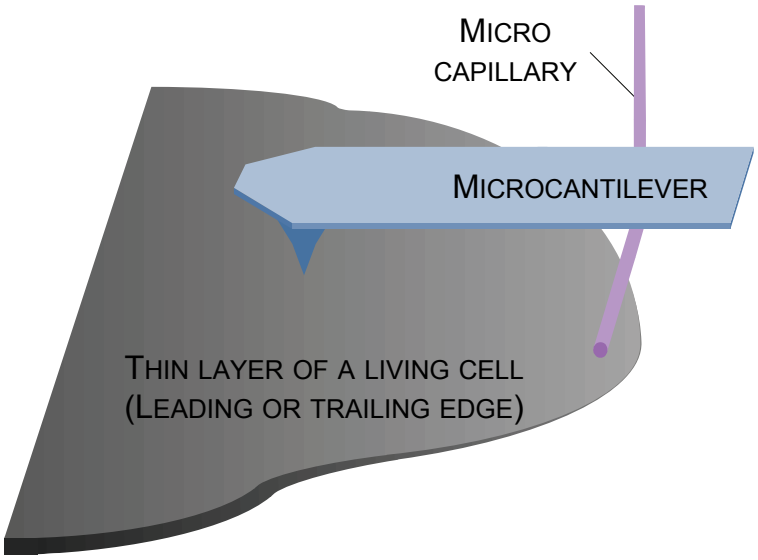

Figure 4.15 Experimental setup for the AFM indentation to characterize an elastic modulus k_{total} of the detached thin layer of fibroblasts. After holding a thin layer with a bent glass microcapillary and then detaching it from a substrate, the detached thin layer is probed with an AFM microcantilever.

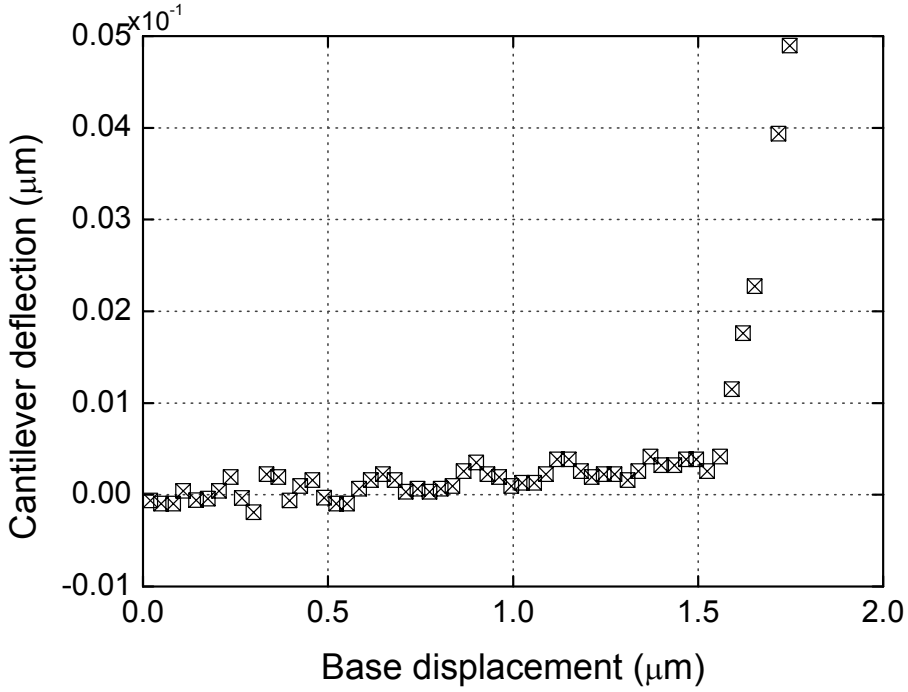

Figure 4.16 Measured cantilever deflection as a function of base displacement for the detached thin layer, showing the elastic modulus is about 1320±310 Pa. The symbols of "+" and "○" of the inset are AFM indentation and cell-holding positions, respectively. Scale bar is 20 μm.

CHAPTER 5. CONCLUSIONS

The cell function of a living cell is known to be regulated by its dynamic behavior (e.g. cellular detachment), a quantitative characterization of which is essential to understand the diverse pathophysical phenomena of inflammatory immune response, wound healing, cancer metastasis, etc. Although an enormous amount of basic research has been made to manipulate cell motility for a better characterization of cellular dynamics, it has showed not quantitative results but qualitative ones. The new biological platforms with exquisite features of addressability, multifunctionality, and reusability in spatiotemporal manipulation of cell motility at cellular and even subcellular levels, biological breadboards, have been designed, microfabricated, and biologically characterized to offer a new method to quantitatively analyze cellular dynamics.

Our biological breadboards composed of M×N gold electrodes, identical and independently operated, on Pyrex glass substrate have been microfabricated by combining optical lithography, e-beam evaporation, and lift-off process to secure the addressability, thereby achieving high-degree-of-freedom in programmably manipulating adherent cell motility. The multifunctionality and reusability of the biological breadboards has been implicated by two-step surface-treatments. The surfaces of the microfabricated biological breadboards have been treated with a polyethylene glycol for the Pyrex glass and a RGD-terminated thiol for the gold electrodes. The first surface-treatment has been done to achieve a cell-resistive surface which suppresses cell adhesion and spreading on the Pyrex glass, whereas the second one has been made to tether the RGD peptide into the gold electrodes via thiol linker, and consequently to achieve a cell-adhesive surface. The biological boards have detached a cell or a part of the cell from their substrate at cellular and subcellular levels using the rapid reductive desorption of a thiol-gold SAM, formed on the gold electrodes through the RGD-terminated thiol surface-treatment, under low bias potential, according to the electrochemical reaction of $R\text{-}S\text{-}Au + H^+ + e^- \rightarrow R\text{-}S\text{-}H + Au$.

In the experimental studies with NIH 3T3 cell line, cellular and subcellular detachments have been successfully demonstrated with the microfabricated biological breadboards both to quantitativelt characterize the cellular (or subcellular) dynamics and to experimentally demonstrate the addressability, multifunctionality, and reusability of the biological breadboards. As an example of the BBBs' biological application, the viscoelastic properties in the motile thin layer of mouse fibroblast NIH 3T3 cells after subcellular detachment have been investigated in an experimental method. The measured results have demonstrated that the method combining the time-sequential images of subcellular retraction with AFM indentation results is ideally suited for measuring the viscoelastic properties of the motile thin layer, thereby leading to a better understanding of cellular dynamics. The biological breadboards are expected to be used to reveal a secret about critical cellular aspects, thereby achieving a remarkable progress of cellular dynamics.

REFERENCES

[1] B. Geiger, A. Bershadsky, R. Pankov, and K. M. Yamada, "Transmembrane crosstalk between the extracellular matrix and the cytoskeleton," *Nature Reviews Molecular Cell Biology*, **2** (2001), 793-805.

[2] R. D. Kamm and M. R. K. Mofrad, "On the molecular basis for mechanotransduction," *Molecular and Cellular Biomechanics*, **1** (2004), 201-209.

[3] D. E. Ingber, "Cellular mechanotransduction: putting all the pieces together again," *The FASEB Journal*, **20** (2006), 811-827.

[4] D. T. Butcher, T. Alliston, and V. M. Weaver, "A tense situation: forcing tumor progression," *Nature Reviews Cancer*, **9** (2009), 108-122.

[5] D. Stamenovic and M. F. Coughlin, "The role of prestress and architecture of the cytoskeleton and deformability of cytoskeletal filaments in mechanics of adherent cells: a quantitative analysis," *Journal of Theoretical Biology*, **201** (1999), 63-74.

[6] T. H. Park and M. L. Shuler, "Integration of cell culture and microfabrication technology," *Biotechnology Progress*, **19** (2003), 243-253.

[7] P. Clark, P. Connolly, A. S. Curtis, J. A. Dow, and C. D. Wilkinson, "Topographical control of cell behaviour: I. Simple step cues," *Development*, **99** (1987), 439-448.

[8] B. Chehroudi, T. R. L. Gould, and D. M. Brunette, "Titanium-coated micromachined grooves of different dimensions affect epithelial and connective-tissue cells differently in vivo," *Journal of Biomedical Materials Research*, **24** (1990), 1203-1219.

[9] J. W. Lussi, C. Tang, P.-A. Kuenzi, U. Staufer, G. Csucs, J. Vörös, G. Danuser, J. A. Hubbell, and M. Textor, "Selective molecular assembly patterning at the nanoscale: a novel platform for producing protein patterns by electron-beam lithography on SiO_2/indium tin oxide-coated glass substrates," *Nanotechnology*, 16 (2005), 1781-1786.

[10] K.-B. Lee, S.-J. Park, C. A. Mirkin, J. C. Smith, and M. Mrksich, "Protein nanoarrays generated by dip-pen nanolithography," *Science*, **295** (2002), 1702-1705.

[11] J. D. Hoff, L.-J. Cheng, E. Meyhöfer, L. J. Guo, and A. J. Hunt, "Nanoscale protein patterning by imprint lithography," *Nano Letters*, **4** (2004), 853-857.

[12] C. S. Chen, M. Mrksich, S. Huang, G. M. Whitesides, and D. E. Ingber, "Geometric control of cell life and death," Science, **276** (1997), 1425-1428.

[13] N. Y. Lee, J. R. Lim, and Y. S. Kim, "Selective patterning and immobilization of biomolecules within precisely-defined micro-reservoirs," *Biosensors and Bioelectronics*, **21** (2006), 2188-2193.

[14] E. A. Roth, T. Xu, M. Das, C. Gregory, J. J. Hickman, and T. Boland, "Inkjet printing for high-throughput cell patterning," *Biomaterials*, **25** (2004), 3707-3715.

[15] J. Lahann, S. Mitragotri, T.-N. Tran, H. Kaido, J. Sundaram, I. S. Choi, S. Hoffer, G. A. Somorjai, and R. Langer, "A reversibly switching surface," *Science*, **299** (2003), 371-374.

[16] A. Folch, B.-H. Jo, O. Hurtado, D. J. Beebe, and M. Toner, "Microfabricated elastomeric stencils for micropatterning cell cultures," *Journal of Biomedical Materials Research*, **52** (2000), 346-353.

[17] A. L. Birkbeck, R. A. Flynn, M. Ozkan, D. Song, M. Gross, and S. C. Esener, "VCSEL arrays as micromanipulators in chip-based biosystems," *Biomedical Microdevices*, **5** (2003), 47-54.

[18] M. Ozkan, T. Pisanic, J. Scheel, C. Barlow, S. Esener, and S. N. Bhatia, "Electro-optical platform for the manipulation of live cells," *Langmuir*, **19** (2003), 1532-1538.

[19] A. Rosenthal and J. Voldman, "Dielectrophoretic traps for single-particle patterning," *Biophysical Journal*, **88** (2005), 2193-2205.

[20] T. Okano, N. Yamada, M. Okuhara, H. Sakai, and Y. Sakurai, "Mechanism of cell detachment from temperature-modulated, hydrophilic-hydrophobic polymer surfaces," *Biomaterials*, **16** (1995), 297-303.

[21] X. Jiang, R. Ferrigno, M. Mrksich, and G. M. Whitesides, "Electrochemical desorption of self-assembled monolayers noninvasively releases patterned cells from geometrical confinements," *Journal of the American Chemical Society*, **125** (2003), 2366-2367.

[22] E. E. Hui and S. N. Bhatia, "Micromechanical control of cell-cell Interactions," *Proceedings of the National Academy of Sciences*, **104** (2007), 5722-5726.

[23] B. Geiger, A. Bershadsky, R. Pankov, and K. M. Yamada, "Transmembrane crosstalk between the extracellular matrix−cytoskeleton crosstalk," *Nature Reviews Molecular cell biology*, **2** (2001), 793-805.

[24] D. Stamenovic and M. F. Coughlin, "The role of prestress and architecture of the cytoskeleton and deformability of cytoskeletal filaments in mechanics of adherent cells: a quantitative analysis," *Journal of Theoretical Biology*, **201** (1999), 63-74.

[25] Karp G, *Cell and molecular biology: concepts and experiments*, American Institute of Chemical Engineers, 2007.

[26] C. A. Widrig, C. Chung, and M. Porter, "The electrochemical desorption of n-alkanethiol monolayers from polycrystalline Au and Ag electrodes," *Journal of Electroanalytical Chemistry and Interfacial Electrochemistry*, **310** (1991), 335-359.

[27] E. Ruoslahti, "RGD and other recognition sequences for integrins," *Annual Review of Cell and Developmental Biology*, **12** (1996), 697-715.

[28] B. T. Houseman and M. Mrksich, "The microenvironment of immobilized Arg-Gly-Asp peptides is an important determinant of cell adhesion," *Biomaterials*, **22** (2001), 943-955.

[29] S. I. Jeon, J. H. Lee, J. D. Andrade, and P. G. De Gennes, "Protein surface interactions in the presence of polyethylene oxide: simplified theory," *Journal of Colloid and Interface Science*, **142** (1991), 149-158.

[30] T. McPherson, A. Kidane, I. Szleifer, and K. Park, "Prevention of protein adsorption by tethered poly(ethylene oxide) layers: experiments and single-chain mean-field analysis," *Langmuir*, **14** (1998), 176-186.

[31] N. P. Desai and J. A. Hubbell, "Solution technique to incorporate polyethylene oxide and other water-soluble polymers into surfaces of polymeric biomaterial," *Biomaterials*, **12** (1991), 144-153.

[32] M. Zhang, T. Desai, and M. Ferrari, "Proteins and cells on PEG immobilized silicon surfaces," *Biomaterials*, **19** (1998), 953-960.

[33] S. P. Palecek, C. E. Schmidt, D. A. Lauffenburger, and A. F. Horwitz, "Integrin

dynamics on the tail region of migrating fibroblasts," *Journal of Cell Science*, **109** (1996), 941-952.

[34] A. J. Ridley, M. A. Schwartz, K. Burridge, R. A. Firtel, M. H. Ginsberg, G. Borisy, J. T. Parsons, and A. R. Horwitz, "Cell migration: integrating signals from front to back," *Science*, **302** (2003), 1704-1709.

[35] A. R. Bausch, W. Möller, and E. Sackmann, "Measurement of local viscoelasticity and forces in living cells by magnetic tweezers," *Biophysical Journal*, **76** (1999), 573-579.

[36] F. Guilak, J. R. Tedrow, and R. Burgkart, "Viscoelastic properties of the cell nucleus," *Biochemical and Biophysical Research Communications*, **269** (2000), 781-786.

[37] C. T. Lim, M. Dao, S. Suresh, C. H. Sow, and K. T. Chew, "Large deformation of living cells using laser traps," *Acta Materialia*, **52** (2004), 1837-1845.

[38] D. P. Theret, M. J. Levesque, M. Sato, R. M. Nerem, and L. T. Wheeler, "The application of a homogeneous half-space model in the analysis of endothelial cell micropipette measurements," *Journal of Biomechanical Engineering*, **110** (1988), 190-199.

[39] D. Shin and K. Athanasiou, "Cytoindentation for obtaining cell biomechanical properties," *Journal of Orthopaedic Research*, **17** (2005), 880-890.

[40] H. Haga, S. Sasaki, K. Kawabata, E. Ito, T. Ushiki, and T. Sambongi, "Elasticity mapping of living fibroblasts by AFM and immunofluorescence observation of cytoskeleton," *Ultramicroscopy*, **82** (2000), 253-258.

[41] H. Haga, M. Nagayama, and K. Kawabata, "Imaging mechanical properties of living cells by scanning probe microscopy," *Current Nanoscience*, **3** (2007), 97-103.